Chapter 4

Conductance-based models

Each neuron is a miniature analog computer. Analog, because its behavior depends on the membrane potential, which is a continuous variable. The information processed by a neuron is via charge-flow across its membrane, which causes changes in its membrane potential, our variable of interest. The charge-flow depends on the conductance of ion channels, which in many cases varies with the membrane potential. The ensuing feedback loops, in which the membrane potential impacts channel-conductance, which in turn impacts membrane potential, give rise to a wealth of exciting and useful dynamical behaviors, such as voltage-spikes, oscillations, and bistability. This chapter focuses on such voltage-dependent single-cell phenomena.

4.1. Introduction to the Hodgkin-Huxley model

In 1952 Alan Hodgkin and Andrew Huxley published a series of five papers [1-5] (the first with Bernard Katz) culminating in their model for the generation and propagation of the action potential by active sodium and potassium channels. Their work combined computational neuroscience with meticulously analyzed electrophysiological data acquired from the giant axon of the squid. Their model, now known as the Hodgkin-Huxley model, will be described in detail in this chapter, because it is the basis for all conductance-based models. In 1963 Hodgkin and Huxley (jointly with John Eccles) received the Nobel Prize for their work, which began the field of computational neuroscience at a time when computers were rarely available—indeed Huxley spent a few weeks carrying out the necessary calculations on a Brunsviga, a hand-operated mechanical calculating machine (Figure 4.1).

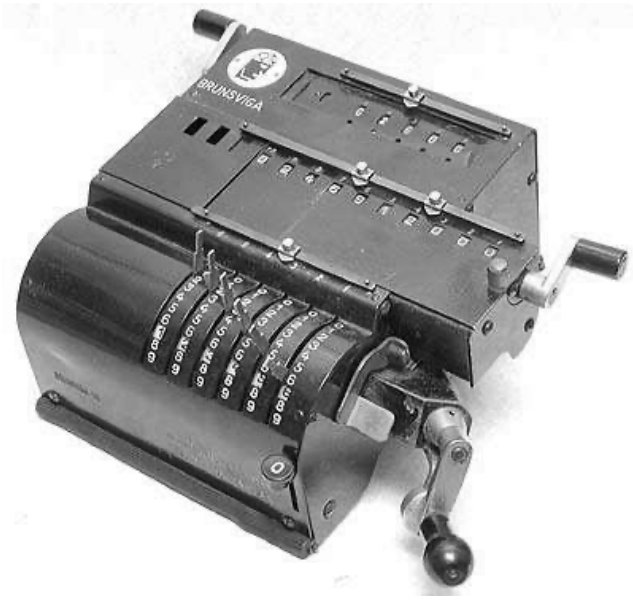

Figure 4.1. A mechanical calculating machine, the Brunsviga, of the type used by Huxley. For each mathematical operation, Huxley would need to set levers in place and turn a crank to produce an answer. The huge amount of effort required to simulate the model equations gave Hodgkin and Huxley the impetus to use sophisticated mathematical methods to minimize the calculation time. Photo from www.vintagecalculators.com, used with permission.

Box 4.1. Electrophysiological data: Refers to measurements of the membrane potential of neurons.

4.1.1. Positive versus negative feedback

While the impressive calculations of Hodgkin and Huxley led to a prediction of the speed of propagation of a spike of voltage called the action potential along the giant squid's axon, we will just model the dynamics of the voltage spike (not its spatial dependence) in this book. The key to the dynamics of a single spike (Figure 4.2) is very fast (sub-millisecond) positive feedback, followed by slow negative feedback. In the mathematical sense, positive or negative says nothing about whether it is good or bad—in fact in most scientific situations positive feedback is a problem (think explosion) while negative feedback is essential (stabilization and control).

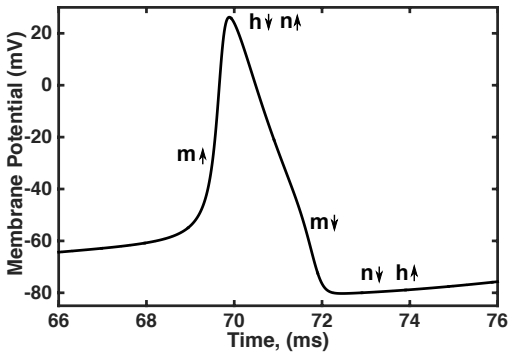

Figure 4.2. Stages of the action potential. a) Sodium activation, m↑, causes a rapid upswing of the membrane potential, V, by opening sodium channels. b) Slower sodium inactivation, h↓, closes sodium channels and potassium activation, n↑, opens potassium channels at high-V to bring about the fall in membrane potential. C) Deactivation of sodium channels, m↓, as V falls below threshold. d) Slower deinactivation of sodium channels, h↑, and deactivation of potassium channels, n↓, at hyperpolarized V

allows V to rise again ready for a new spike. This figure is produced by the online code `HH_old_base.m`.

In terms of the action potential, positive feedback means that as the membrane potential increases, a biophysical process comes into play that acts to further increase the membrane potential. In this case, it is the voltage-dependent activation of sodium channels: channels open as the membrane potential rises and their opening admits an influx of positive sodium ions to the cell, which raises the membrane potential further. In principle, sodium activation can raise the membrane potential to a level as high as the sodium reversal potential, the point at which the sodium current would fall to zero however large the sodium conductance. However, typically before that point is reached, negative feedback comes into play.

Box 4.2. Channel activation: a membrane potential-dependent process necessary for the opening of a channel, usually by depolarization.

Box 4.3. Channel deactivation: the opposite of channel activation, usually by hyperpolarization.

Box 4.4. Channel inactivation: A process that occurs with depolarization to prevent channels from opening.

Box 4.5. Channel deinactivation: The opposite of inactivation, a process that is necessary for a channel to open, with the opposite voltage-dependence of activation.

Negative feedback arises through three mechanisms. The first, a reduction in sodium current as its reversal is approached, is not that important in shaping the action potential—sodium reversal ensures a spike has a maximum height, but cannot bring the membrane potential back to baseline. That process depends on sodium inactivation and potassium activation, which will be described below.

On the one hand, sodium channels inactivate with depolarization of the membrane potential. Ions cannot flow through an inactivated channel. Inactivation is slower than activation so that as the membrane potential is shifted from low to high, the channels are activated (allowing current flow) for a short period of time before they inactivate (preventing current flow). This means the sodium current is a transient current—it is not maintained at high levels if the membrane potential is held fixed, even far below sodium's reversal potential. Inactivation of the sodium channels alone would allow the membrane potential to decay back to rest at the leak potential, but slowly over a time on the order of 10ms that corresponds to the neuron's base time constant ($\tau_m = C_m R_m$).

Box 4.6. Transient current: A current through an ion channel that rises and decays when the membrane potential is changed, but does not persist.

Box 4.7. Delayed rectifier current: The outward potassium current that activates more slowly than the sodium current and acts to terminate a spike by returning the membrane potential back to baseline.

However, real action potentials are much sharper, with a much more rapid return of the membrane potential to its resting level thanks to the opening of potassium channels. Like sodium channels, the potassium channels activate with increasing membrane potential. They are slower to activate though, permitting the initial peak in membrane potential before they start dominating and producing an outward current. The greater the peak potassium conductance, the more rapidly charge flows back out of the neuron and the narrower the voltage spike. These potassium channels are known as delayed rectifier channels. They are called delayed because their slower responsiveness means their full effect is delayed compared to the more rapid sodium activation. The term rectifier is added because the channels only open when the membrane potential is above the reversal potential for potassium, allowing for an outward, unidirectional or 'rectifying', flow of current. Unlike sodium channels, the potassium delayed-rectifier channels do not inactivate, so they produce a persistent conductance—if the voltage is clamped at a depolarized level, the conductance (and hence the outward current) is sustained.

Although these spike-producing processes were uncovered in the axon of the Giant Squid, the biophysical processes are the same as those producing the action potentials in our own brains. The main difference when looking at spikes in mammalian cortex, for example, is the spike width being sub-millisecond due to faster channel kinetics.

4.1.2. Voltage clamp versus current clamp

When studying neurons, one often controls the applied current and observes the dynamics of the membrane potential in what is called current-clamp mode. Alternatively, one can control the membrane potential and observe the voltage-dependent dynamics of currents and conductances in voltage-clamp mode. The voltage-clamp approach is useful, or even essential, in electrophysiological experiments that attempt to uncover the behavior of a particular conductance. In particular, it underlay the process by which Hodgkin and Huxley deduced the dynamics of the gating variables in their original model.

Box 4.8. Voltage clamp: Measurements of the current flowing into or out of a neuron when its membrane potential is controlled in an experiment.

Box 4.9. Current clamp: Measurements of the changes in the membrane potential of a neuron when its input current is controlled in an experiment.

In real neurons, some skill is needed to ensure the membrane potential is clamped to the same value throughout the cell in voltage-clamp mode. However, in simulations one need only pre-assign the value of the membrane potential at each time point and remove the membrane potential update step from the code. When building up a simulation of a neuron, it is worth testing the behavior of each added conductance in voltage-clamp mode, to ensure it acts as it should, before simulating the full dynamics of the membrane potential.

4.2. Simulation of the Hodgkin-Huxley model

The Hodgkin-Huxley model is based on four variables: membrane potential, V_m; sodium activation variable, m; sodium inactivation variable, h; and potassium activation variable,

n. Therefore, four coupled differential equations are simulated to produce the dynamics of the model. The activation and inactivation variables are together called gating variables, because they characterize whether the corresponding channels are open or shut (*i. e.*, able to pass ionic current). Each gating variable has a voltage-dependent steady-state value that it would reach if the membrane potential were fixed. Each also has a voltage-dependent time constant, which determines the rate at which it approaches that steady state.

Box 4.10. Gating variable: A variable between 0 and 1, representing the fraction of channels in a particular state. Multiplication together of all such variables for a type of channel indicates the fraction of the channels that are open and able to transmit current.

For many channel-types these voltage-dependent functions are obtained by direct fitting to empirical data. Hodgkin and Huxley went further by deriving rate constants and fitting functions to those rate constants. The connection between steady state values and time constants with the underlying rate constants is best understood by consideration of a two-state system.

4.2.1. Two-state systems

A simple, but very important system in biology is one of many identical components, each of which can be in one of two states. Here we call the states A and B with rate constants k_A for the switch from B to A and k_B for the switch from A to B:

$$A \underset{k_A}{\overset{k_B}{\rightleftharpoons}} B \qquad \text{Eq. 4.1}$$

To be concrete, we can assume A and B to be two conformational states of a particular protein. Then we will use lower-case a and b to represent the fraction of protein molecules in states A and B respectively. Clearly a and b (like the gating variables we are considering in the Hodgkin-Huxley model) can vary in the range from 0 to 1. Also, in a two-state system, all protein molecules are in either state A or state B, so we have the constraint

$$a + b = 1$$

or equivalently

$$b = 1 - a.$$

The rate constants give the rate of change of a and b from first-order reaction kinetics in chemistry as

$$\frac{da}{dt} = k_A b - k_B a = k_A(1 - a) - k_B a \qquad \text{Eq. 4.2}$$

$$\frac{db}{dt} = -k_A b + k_B a = -k_A b + k_B(1 - b). \qquad \text{Eq. 4.3}$$

We will just consider Eq. 4.2, because Eq. 4.3 is essentially identical, and if we know the dynamics of a we can just set $b = 1 - a$ to obtain the dynamics of b.

First, we can find the steady state of a (a_∞) by solving $\frac{da}{dt} = 0$ in Eq. 4.2, which leads to

$$k_A(1 - a_\infty) - k_B a_\infty = 0 \qquad \text{Eq. 4.4}$$

and after rearranging,

$$a_\infty = \frac{k_A}{k_A + k_B}. \qquad \text{Eq. 4.5}$$

Eq. 4.5 produces the expected behavior, with the steady state of a ranging from near zero when rate of transition away from A is much greater than rate of transition to A (*i. e.,* when $k_B \gg k_A$, $a_\infty \to 0$) or to near one when rate of transition to A is much greater than rate of transition away from A (*i. e.,* when $k_A \gg k_B$, $a_\infty \to 1$).

The time constant, τ_a, for the dynamical process can be evaluated by rewriting the first order linear differential equation in the form

$$\frac{da}{dt} = \frac{a_\infty - a}{\tau_a} \qquad \text{Eq. 4.6}$$

(see Section 1.4.1).

To extract the time constant, one notices that the prefactor of a in Eq. 4.6 is $\frac{-1}{\tau_a}$ so equating this with the prefactor of a in Eq. 4.2 yields

$$\frac{-1}{\tau_a} = -k_A - k_B,$$

which leads to

$$\tau_a = \frac{1}{k_A + k_B}. \qquad \text{Eq. 4.7}$$

Thus, given rate constants, k_A and k_B, one can calculate steady state, a_∞, and time constant, τ_a. Similarly, given the steady state and time constant, the rate constants can be evaluated from Eqs. 4.5 and 4.7 as:

$$k_A = \frac{a_\infty}{\tau_a} \text{ and } k_B = \frac{1 - a_\infty}{\tau_a}. \qquad \text{Eq. 4.8}$$

In the Hodgkin-Huxley model, the two rate constants for each gating variable are voltage-dependent.

4.2.2. Full set of dynamical equations for the Hodgkin-Huxley model

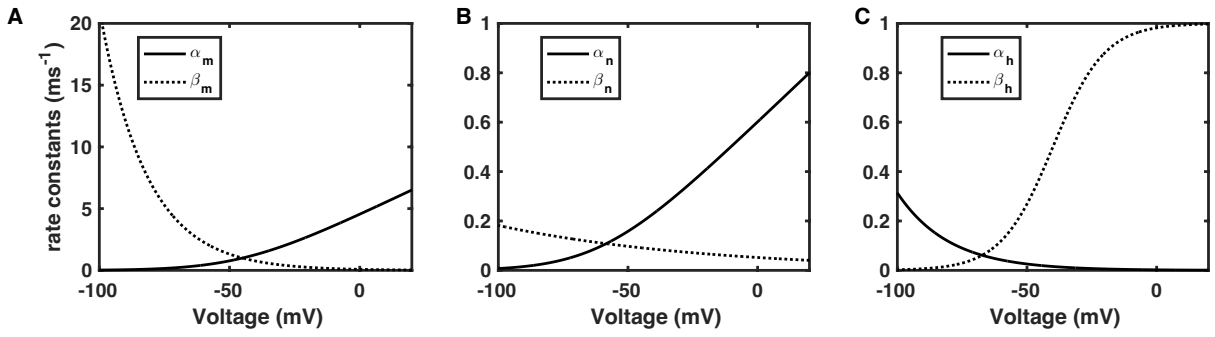

Figure 4.3. Rate constants for the gating variables of the Hodgkin-Huxley model. **A.** Rates of sodium activation, α_m, and deactivation, β_m. **B.** Rates of potassium activation, α_n, and deactivation, β_n. **C.** Rates of sodium deinactivation, α_h, and inactivation, β_h. Note the 20-fold increase in the y-axis scale for the activation variable of sodium, which responds most rapidly. Equations are provided in Table 4.2. This figure was produced by the online code `HHab_plotnewV.m`.

The membrane potential of the Hodgkin-Huxley model follows the dynamical equation

$$C_m \frac{dV_m}{dt} = G_L(E_L - V_m) + G_{Na}^{(max)} m^3 h(E_{Na} - V_m) + G_K^{(max)} n^4 (E_K - V_m) + I_{app} \quad \text{Eq. 4.9}$$

which is like the dynamical equation for the leaky integrate-and-fire model (Eq. 2.9), but with the two extra (middle) terms on the right-hand side, one for the sodium conductance and the other for the potassium conductance. Those conductance terms include the gating variables, m for sodium activation, h for sodium inactivation, and n for potassium activation. The exponents for each gating variable were obtained by fitting to the time-dependence of data long before the biophysical interpretation of the gating variables was established. Intriguingly the potassium delayed-rectifier channel contains four subunits: If each subunit opens independently with a probability of n then the expected fraction of channels with all 4 subunits in the open state is n^4, providing a plausible account for that term in the total potassium conductance. However, in general the channel proteins have many more states and these equations are best considered as an empirical fit.

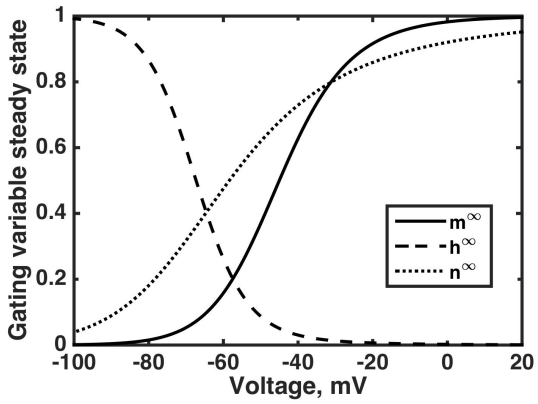

Figure 4.4. Steady state of the gating variables in the Hodgkin-Huxley model. The activation variables approach 1 at positive membrane potentials, whereas the inactivation variable approaches one at very negative membrane potentials. The small region where sodium activation, m, and inactivation, h, are greater than zero provides a voltage "window" in which a sodium current may be sustained. Hence the sodium current can be called a "window current". This figure was produced by the online code `HHab_plotnewV.m`.

Each gating variable follows its own voltage-dependent dynamical equation, in which we use the symbol α as the rate constant for increase of that gating variable and the symbol β as the rate constant for its decrease. The three equations then have identical forms (see prior section):

$$\frac{dm}{dt} = \alpha_m(1 - m) - \beta_m m \quad \text{Eq. 4.10}$$

$$\frac{dh}{dt} = \alpha_h(1 - h) - \beta_h \mathrm{h} \quad \text{Eq. 4.11}$$

$$\frac{dn}{dt} = \alpha_n(1 - n) - \beta_n n \quad \text{Eq. 4.12}$$

but the rate constants have different voltage dependences. In particular, for sodium activation, α_m increases whereas β_m decreases with depolarization; for potassium activation, α_n and β_n have similar voltage-dependences but are smaller, leading to slower dynamics than sodium activation; for sodium inactivation, α_h decreases whereas β_h increases with depolarization, leading to the opposite dependence on the membrane potential for the activation and inactivation gating variables (Figures 4.3 and 4.4).

When the voltage-dependence of the rate constants are known, as in Table 4.2, then the set of Equations 4.9-4.12 can be simulated together (Figures 4.5-4.6) to show the

membrane potential's response to any time-dependent input current, I_{app}. The following section describes the different behaviors produced by such simulations.

4.2.3. Dynamical behavior of the Hodgkin-Huxley model: A Type-II neuron.

Box 4.11. Type-II neuron: A neuron with a discontinuous jump in its firing rate curve and which can be either inactive or active in a history-dependent for some values of input current.

In this section, we consider those behaviors of the Hodgkin-Huxley model that are specific to Type-II neurons. All of these behaviors are symptomatic of sub-threshold oscillations: 1) A jump from a single spike, or unsustained firing, to a high firing rate; 2) Bistability (two possible firing rates for the same input current); 3) Spike generation via hyperpolarization (also called anode break); and 4) Resonance in response to oscillating input currents of different frequencies.

Box 4.12. Subthreshold oscillations: Oscillations in the membrane potential, of insufficient amplitude to produce a spike.

Box 4.13. Bistability: The existence of two stable states of activity, such as spiking and quiescence, at for the same value of all inputs and other parameters.

Box 4.14. Anode break: A spike in the membrane potential produced following release from hyperpolarization.

Box 4.15. Resonance: An enhancement in the response of a system when it is stimulated at a particular frequency, called its resonant frequency.

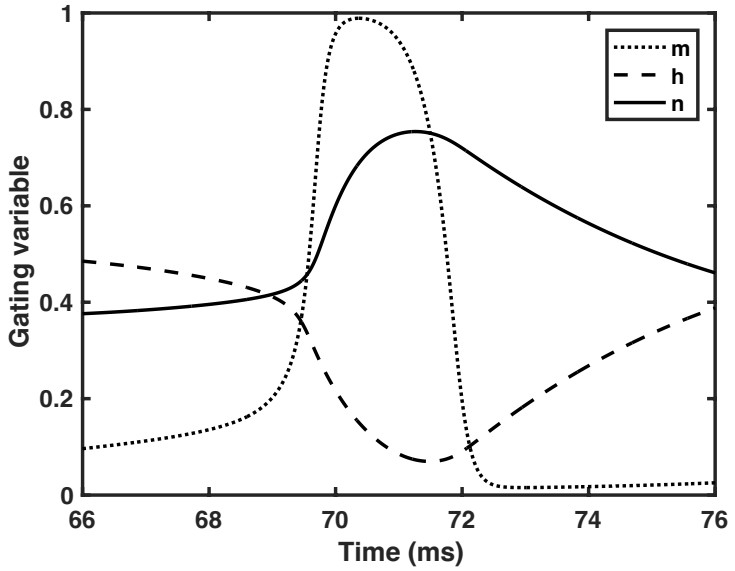

Figure 4.5. Dynamics of gating variables during a single spike. In this example (as in Figure 4.2) the peak of the spike is at 70ms, almost simultaneous with the peak of sodium activation, m (dotted). Sodium inactivation, h (dashed) reaches a minimum and potassium activation, n (solid) reaches a maximum over 1ms later. The neuron is not able to spike again until h and m have increased and n has decreased back to near baseline. This figure is

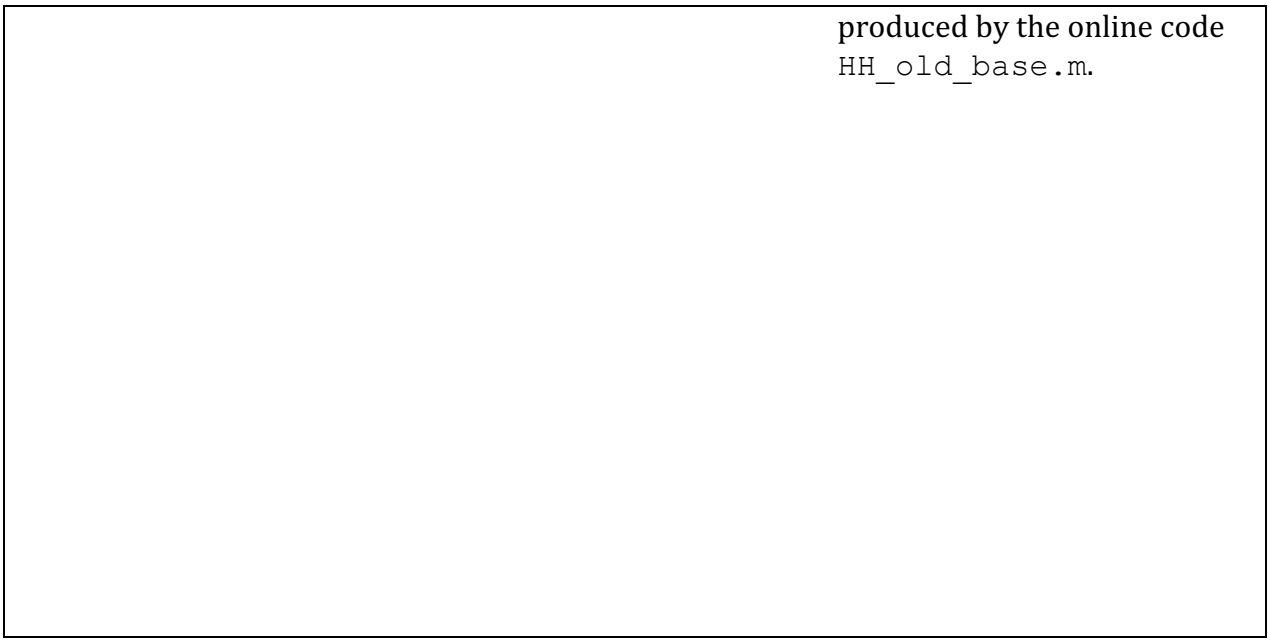

If the Hodgkin-Huxley model is simulated with step currents of different amplitudes (Figure 4.6), a level of input is reached at which a single spike is produced, followed by decaying sub-threshold oscillations. At a higher level of input continuous spiking arises, but the frequency of spiking is never lower than that of the sub-threshold oscillations. Therefore, the f-I curve contains a jump up from zero to a significant firing rate at the current threshold (Figure 4.7). In fact, the vertical line in the figure, which guides the eye, should strictly be omitted, since it passes through values of firing rate that can never be attained by the neuron. Such a discontinuity in the firing rate response defines the Type-II class of neurons.

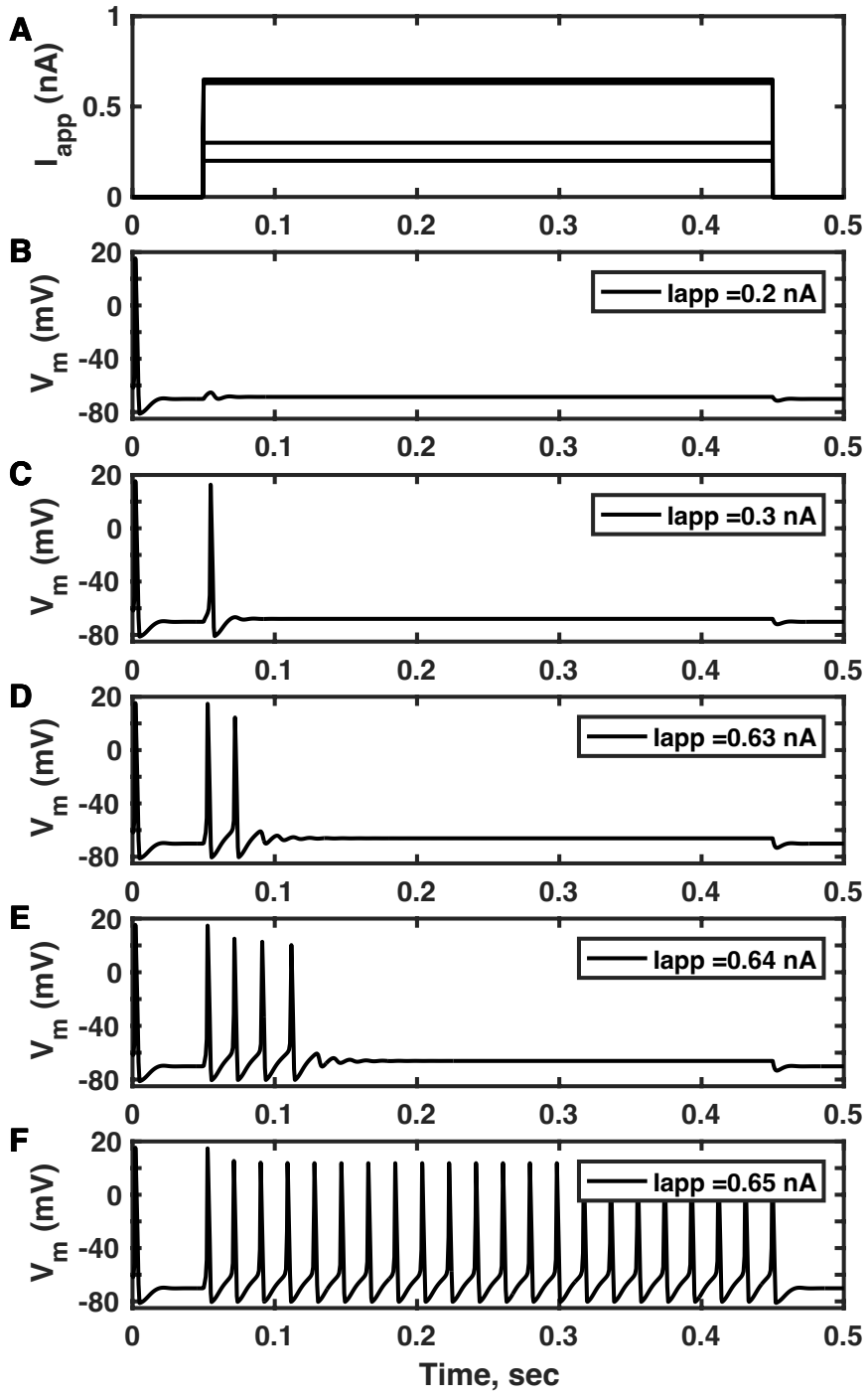

Figure 4.6. Type-II behavior of the Hodgkin-Huxley model. A) Current steps that are applied in panels B)-E). **B)** A 0.2nA applied current produces a decaying sub-threshold oscillation in the membrane potential. **C)** A 0.3nA applied current produces a single spike followed by decaying sub-threshold oscillations. **D)** A 0.63nA applied current produces two spikes, the second of lower amplitude than the first, followed by more slowly decaying subthreshold oscillations. **E)** A 0.64nA applied current produces a succession of 4 spikes of near constant inter-spike interval, but not sustained firing. Subthreshold oscillations follow the last spike. **F)** An applied current of 0.65nA is just sufficient to produce sustained spiking, but at a high frequency of over 50Hz. This figure is produced by the online code `HH_manyItrials.m`.

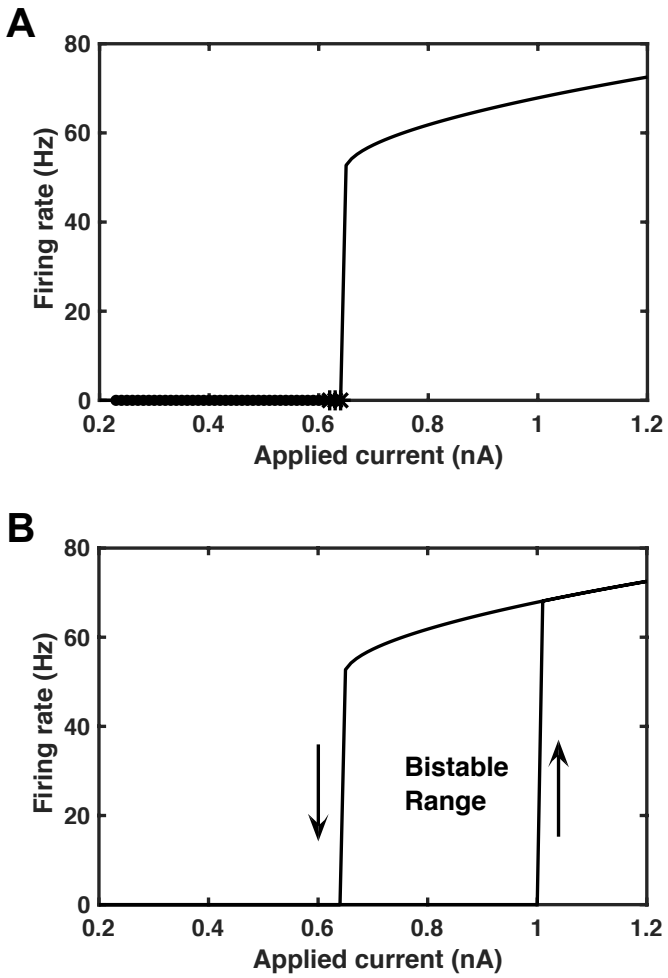

Figure 4.7. Firing rate curve of Hodgkin-Huxley model. A. Firing rate in response to current steps from a baseline of 0nA, as used in Figure 4.5. Small solid circles indicate a single spike is produced; crosses indicate multiple spikes are produced without sustained firing. **B.** Firing rate in response to a protocol of current steps that successively increase from the previous value without reset, then successively decrease. For a wide range of currents the system is bistable, with the neuron remaining quiescent (zero firing rate) if initially quiescent, or sustaining firing if spiking is already initiated. The code used to generate this figure can be found online as `HH_new_f_I_bi.m`.

Moreover, one must take care in plotting an f-I curve, as the neuron's spiking behavior at a given level of applied current is history-dependent (Figure 4.7, lower panel). For example, if the applied current is gradually increased a much higher applied current is needed for the neuron to produce an action potential than if the current were stepped up instantaneously from zero.

To understand the history-dependence, we first recall that the neuron can produce a spike because the positive feedback of sodium activation is much more rapid than the negative feedback of sodium inactivation and potassium activation. However, if the membrane potential is raised incrementally then the negative feedback terms have time to become stronger so that the membrane potential (and hence the applied current) must be higher before sodium activation can dominate and "take off".

Conversely, once the neuron is producing spikes, a lower value of applied current is needed to maintain further spikes. This is because, following each spike, sodium channels are more deinactivated (higher h) and potassium channels are more deactivated (lower n) than the steady state level produced by gradual increment of the applied current. Both sodium deinactivation and potassium deactivation make it easier for the neuron to produce

a new spike by sodium activation. That is, whether a spike is produced at a given level of applied current or depolarization depends on the state of variables—in particular of sodium inactivation, h, and potassium activation, n—not just on the membrane potential alone.

A second example of the need to consider more than the membrane potential is the demonstration of the "anode break" action potential (Figure 4.8). In this case, the Hodgkin-Huxley model neuron produces a single spike when the applied current is returned to zero following a period of hyperpolarization. Such a feature of the Hodgkin-Huxley model and other type-II neurons is impossible in an integrator model of a neuron, such as the leaky integrate-and-fire. However, when we think of the neuron as an oscillator the behavior becomes more understandable.

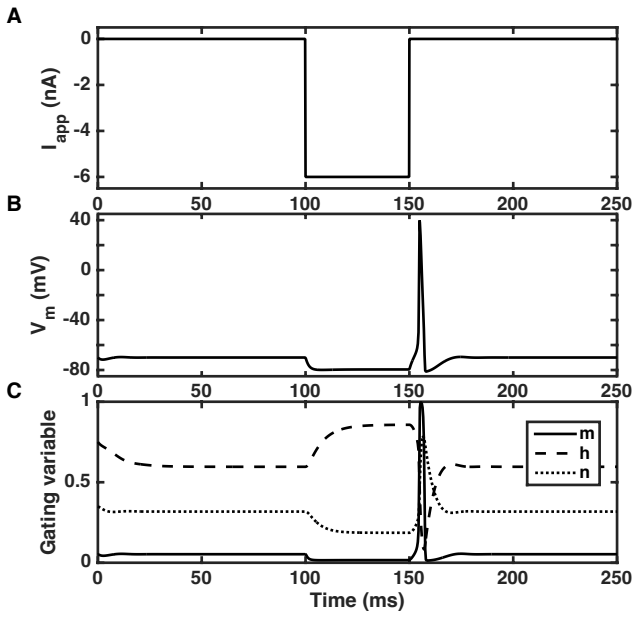

Figure 4.8. Anode break, a spike from hyperpolarization. A) Applied current is negative (outward and hyperpolarizing) for a period of 50ms. **B)** When the applied current is released and returns abruptly to its baseline value of zero an action potential is produced. **C)** A plot of the gating variables reveals that the period of hyperpolarization increased the inactivation variable, h, in a process called deinactivation. In combination with a reduced potassium conductance due to the reduction in potassium activation, n, the deinactivation dramatically reduces the threshold for a sodium spike. This figure was produced by the online code `HH_old_anode_break_3plot.m`.

For example, instead of pushing a swing to get it going, one can pull backward then release the swing. Mathematically the same is occurring when a negative current is applied to the neuron, which is then released. The key for the neuron is the process of deinactivation of sodium—the inactivation variable, h, approaches its maximum, 1, upon hyperpolarization, making a spike easier—combined with deactivation of potassium—the potassium activation variable, n, approaches zero upon hyperpolarization, reducing the potassium current that counteracts any sodium spike.

These behaviors show that the notion of a threshold for spiking as used in the simplest leaky integrate-and-fire models is purely a simplification and convenience. It should not be taken literally in more realistic models, yet alone in real neurons. Whether a model neuron produces a spike depends on the combination of all of the variables in the model, so when the variables change at different rates, production of a spike is history-dependent. Since electrophysiological experiments do not allow for measurement of gating

variables, it is common to plot the membrane potential, V_m, against its time-derivative, dV_m/dt, to gain at least one extra factor in determining whether an action potential should be produced.

The subthreshold oscillations underlying much of the Type-II behavior can be observed following a step current that is just insufficient to produce an action potential (Figure 4.9). In the Hodgkin-Huxley model these oscillations are strongly damped, meaning they decay rapidly. It is possible to observe sustained subthreshold oscillations in real neurons and in other models, though usually at a lower frequency due to the presence of other currents. Complete removal of the subthreshold oscillations transforms a Type-II neuron into a Type-I neuron, which possesses none of the features discussed here. In the next section, we will add an extra potassium current to produce the Connors-Stevens model, which exhibits such Type-I behavior.

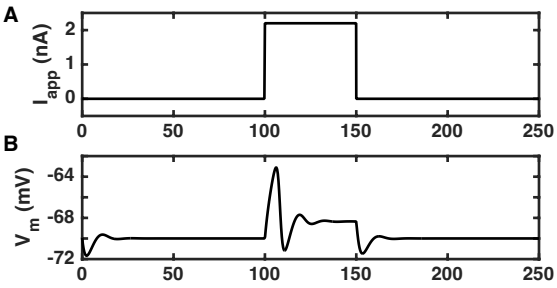

Figure 4.9. Subthreshold oscillations following step changes in current. A) A subthreshold step of current is applied for 50ms. **B)** The membrane potential responds with a brief period of damped oscillations.

Box 4.16. Type-I neuron: a neuron whose firing rate increases from zero without any rate-jump as input current is incrementally increases above threshold.

A final property of intrinsic oscillators is their resonant response to non-uniform applied currents. Resonance is a ubiquitous feature of oscillating systems. Resonance means that the system responds most strongly to inputs that match its natural frequency. We all know that when pushing a swing we must time successive pushes to get it higher and that if we push at the wrong time we can slow the swing down and stop it.

In neurons, resonance can be observed in the response to a frequency sweep of oscillating applied current [6] known as the ZAP protocol (ZAP for impedance amplitude profile, where Z is the symbol in physics for impedance, which is proportional to resistance but includes phase). Figure 4.10 demonstrates the results of such a protocol applied to the Hodgkin-Huxley model using two different amplitudes for the peak of the oscillating applied current. Whereas the applied current oscillations have constant amplitude, the neuron's response peaks at intermediate frequencies—approximately at the frequency of the subthreshold oscillations. In Figure 4.10C, the stronger response in a particular frequency range leads the model neuron to produce spikes only when the input frequency is near the neuron's natural frequency—its resonant frequency.

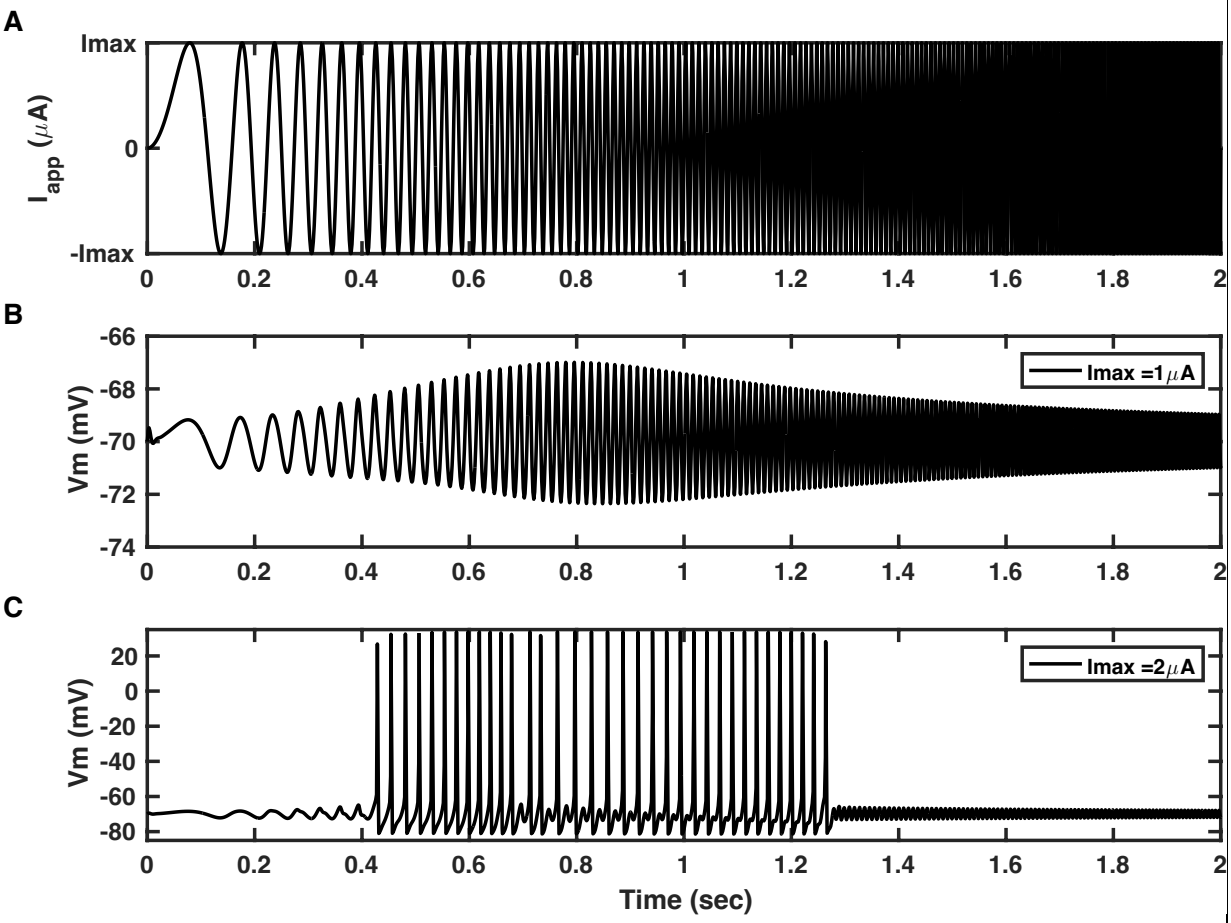

Figure 4.10. Resonant response to a frequency sweep or "ZAP" current. Top: The injected current is given by a sine wave of linearly increasing frequency: $I_{app}(t) = I_{max}\sin[2\pi f(t)\cdot t]$ where $f(t) = f_0 + (f_{max} - f_0)\,t/t_{max}$, $f_0 = 0$Hz, $f_{max} = 80$Hz and $t_{max} = 2$s. **Center:** With $I_{max} = 0.1n$A, the membrane potential oscillates in response at the same frequency as the applied current, with an amplitude that peaks near 0.8s when the frequency is 32Hz. **Bottom:** With $I_{max} = 0.2n$A, the membrane potential responds with action potentials when the oscillation frequency is within the resonant range. Notice that at the resonant frequency for subthreshold oscillations (at a time near 0.8s) the neuron spikes on alternate current peaks because it takes the neuron longer to recover from the large deviation of a spike (bottom) than the smaller subthreshold oscillation (center). This figure can be produced by the code `HH_new_zap.m`.

In Tutorial 4.1 we will see how the time spacing of short current pulses can determine whether a spike is initiated and conversely how sustained spiking can be ended with a positive current pulse at just the right time.

Table 4.1. Parameter values for H-H model (Figures 4.2-4.10 and Tutorial 4.1).		
Parameter	Symbol	Value *
Leak conductance	G_{Leak}	30nS
Maximum sodium conductance	$G_{Na}^{(max)}$	12μS
Maximum delayed rectifier conductance	$G_{K}^{(max)}$	3.6μS
Sodium reversal potential	E_{Na}	45mV
Potassium reversal potential	E_K	-82mV
Leak reversal potential	E_L	-60mV
Membrane Capacitance	C_m	100pF
Applied current	I_{app}	Variable

* Assumes a total membrane area of 0.1mm^2.

Table 4.2. Gating variables of the H-H model (Figures 4.2-4.10 and Tutorial 4.1).			
Gating variable	Steady state	Time Constant	Rate constants
m	$\frac{\alpha_m}{\alpha_m + \beta_m}$	$\frac{1}{\alpha_m + \beta_m}$	$\alpha_m = \frac{10^5(-V_m - 0.045)}{\exp[100(-V_m - 0.045)] - 1}$ $\beta_m = 4 \times 10^3 \exp\left[\frac{(-V_m - 0.070)}{0.018}\right]$
h	$\frac{\alpha_h}{\alpha_h + \beta_h}$	$\frac{1}{\alpha_h + \beta_h}$	$\alpha_h = 70 \exp[50(-V_m - 0.070)]$ $\beta_h = \frac{10^3}{1 + \exp[100(-V_m - 0.040)]}$
n	$\frac{\alpha_n}{\alpha_n + \beta_n}$	$\frac{1}{\alpha_n + \beta_n}$	$\alpha_n = \frac{10^4(-V_m - 0.060)}{\exp[100(-V_m - 0.060)] - 1}$ $\beta_n = 125 \exp\left[\frac{(-V_m - 0.070)}{0.08}\right]$

4.3. Tutorial 4.1. The Hodgkin-Huxley model as an oscillator.

In this tutorial, you will simulate a full 4-variable model similar to the original Hodgkin-Huxley model (though using modern units). The four variables, sodium activation, m, sodium inactivation, h, potassium activation, n, and membrane potential, V, will all be

updated on each time step as they depend on each other. Initial conditions should be 0 for all gating variables and E_L for the membrane potential, unless otherwise stated.

a) Set up a simulation of 0.35s duration of the Hodgkin-Huxley model as follows:

$$C_m \frac{dV_m}{dt} = G_L(E_L - V_m) + G_{Na}^{(max)} m^3 h(E_{Na} - V_m) + G_K^{(max)} n^4 (E_K - V_m) + I_{app}$$

$$\frac{dm}{dt} = \alpha_m(1 - m) - \beta_m m$$

$$\frac{dh}{dt} = \alpha_h(1 - h) - \beta_h h$$

$$\frac{dn}{dt} = \alpha_n(1 - n) - \beta_n n$$

where the parameters are given in Table 4.1 and the rate constants are the instantaneous functions of membrane potential given in Table 4.2.

Initially set the applied current to zero and check the membrane potential stabilizes at -70.2mV.

b) Produce a vector for the applied current that has a baseline of zero and steps up to 0.22nA for a duration of 100ms beginning at a time of 100ms. Plot the applied current on an upper graph and the membrane potential's response on a lower graph of the same figure. (You should see subthreshold oscillations but no spikes).

c) Alter your code so that the applied current is a series of 10 pulses, each of 5ms duration and 0.22nA amplitude. Create a parameter that defines the delay from the onset of one pulse to the onset of the next pulse. Adjust the delay from a minimum of 5ms up to 25ms and plot applied current and membrane potential as in b) for two or three examples of pulse separations that can generate spikes. Be careful (especially if using the Euler method) to repeat your simulation with your time step reduced by a factor of 10 to ensure you see no change in the response, as a sign you have sufficient accuracy in the simulation. (A time-step of as low as 0.02μs may be necessary.) Describe and explain your findings.

d) Now set the baseline current to be 0.6nA. Set the initial conditions as $V_m(0) = -0.065\text{V}, m(0) = 0.05, h(0) = 0.5, n(0) = 0.35$. (Note that the "0" in parenthesis indicates a time of $t = 0$, which corresponds to element number 1 in an array.) Apply a series of 10 inhibitory pulses to bring the applied current to zero for a duration 5ms, with pulse onsets 20ms apart. Plot the applied current and the membrane potential's response as in b)-c). Describe and explain what you observe.

e) Now set the baseline current to 0.65nA. Set the initial conditions as $V_m(0) = -0.065\text{V}, m(0) = 0.05, h(0) = 0.5, n(0) = 0.35$. Increase the excitatory current to 1nA for a 5ms pulse at the time point of 100ms. Plot the applied current and resulting behavior in the same manner as b)-d). Describe what occurs and explain your observation.

f) Repeat e) with the baseline current of 0.65nA, but set the initial conditions as $V_m(0) = -0.065\text{V}, m(0) = 0, h(0) = 0, n(0) = 0$. As in e), increase the excitatory current to 1nA for a 5ms pulse at the time point of 100ms. Plot the applied current and resulting behavior in the same manner as b)-e). Describe what

occurs and explain your observation, in particular by comparing with your results to part e).

4.4. The Connor-Stevens Model (a Type-I model).

Table 4.3. Parameter values for the Connor-Stevens model (Figure 4.11).

Parameter	Symbol	Value *
Leak conductance	G_{Leak}	30nS
Maximum sodium conductance	$G_{Na}^{(max)}$	12μS
Maximum delayed rectifier conductance	$G_{K}^{(max)}$	2μS
Maximum A-type conductance	$G_{A}^{(max)}$	4.77μS
Sodium reversal potential	E_{Na}	55mV
Potassium reversal potential	E_K	-72mV
Reversal of A-type channels	E_A	-75mV
Leak reversal potential	E_L	-17mV
Membrane Capacitance	C	100pF
Applied current	I_{app}	Variable

Box 4.17. A-current, I_A: The A-current is an outward (hyperpolarizing) potassium current, which activates at low membrane potentials and inactivates at high membrane potentials. It does not fully deactivate at resting potentials, where it can provide a sufficient outward current to counteract rebound spikes.

The Connor-Stevens model [7] is a variant of the Hodgkin-Huxley model with altered parameters and an additional potassium current called the A-current. The model is designed to reproduce the responses of typical cells in mammalian cortex, which are able to produce spikes at low firing rates, unlike the giant squid neuron that underlies the Hodgkin-Huxley model. The extra potassium current has both activation (a) and inactivation (b) variables (Figure 4.11), so the Connor-Stevens model is a six-variable model that looks very similar to the Hodgkin-Huxley model:

$$C\frac{dV}{dt} = G_L(E_L - V) + G_{Na}^{(max)}m^3h(E_{Na} - V) + G_K^{(max)}n^4(E_K - V) + G_A^{(max)}a^3b(E_A - V) + I_{app} \quad \text{Eq. 4.13}$$

$$\frac{dm}{dt} = \alpha_m(1-m) - \beta_m m \quad \text{Eq. 4.14}$$

$$\frac{dh}{dt} = \alpha_h(1-h) - \beta_h h \quad \text{Eq. 4.15}$$

$$\frac{dn}{dt} = \alpha_n(1-n) - \beta_n n \quad \text{Eq. 4.16}$$

$$\frac{da}{dt} = \frac{a_\infty - a}{\tau_a} \quad \text{Eq. 4.17}$$

$$\frac{db}{dt} = \frac{b_\infty - b}{\tau_b} \quad \text{Eq. 4.18}$$

Table 4.4. Gating variables of the Connor-Stevens model (Figure 4.11).

Gating variable	Steady state	Time Constant	Voltage-dependent variables
m	$\frac{\alpha_m}{\alpha_m + \beta_m}$	$\frac{1}{\alpha_m + \beta_m}$	$\alpha_m = \frac{3.8 \times 10^5 (V + 0.0297)}{1 - \exp[-100(V + 0.0297)]}$ $\beta_m = 1.52 \times 10^4 \exp[-55.6(V + 0.0547)]$
h	$\frac{\alpha_h}{\alpha_h + \beta_h}$	$\frac{1}{\alpha_h + \beta_h}$	$\alpha_h = 266\exp[-50(V + 0.048)]$ $\beta_h = \frac{3800}{1 + \exp[-100(V + 0.018)]}$
n	$\frac{\alpha_n}{\alpha_n + \beta_n}$	$\frac{1}{\alpha_n + \beta_n}$	$\alpha_n = \frac{2 \times 10^4 (V + 0.0457)}{1 - \exp[-100(V + 0.0457)]}$ $\beta_n = 250\exp[-12.5(V + 0.0557)]$
a	a_∞	τ_a	$\tau_a = 3.632 \times 10^{-4} + \frac{1.158 \times 10^{-3}}{1 + \exp[49.7(V + 0.05596)]}$ $a_\infty = \left\{\frac{0.0761\exp[31.4(V + 0.09422)]}{1 + \exp[34.6(V + 0.00117)]}\right\}^{1/3}$
b	b_∞	τ_b	$b_\infty = \left\{\frac{1}{1 + \exp[68.8(V + 0.0533)]}\right\}^4$ $\tau_b = 1.24 \times 10^{-3} + \frac{2.678 \times 10^{-3}}{1 + \exp[62.4(V + 0.050)]}$.

In Eqs. 4.17-4.18, the gating variables for the A-current are just described in terms of their voltage-dependent steady states (a_∞, b_∞) and voltage-dependent time constants (τ_a, τ_b) without an attempt to derive the corresponding rate constants. The standard parameters

for the model are given in Table 4.3 (where a neuron of surface area 0.01mm^2 is assumed). The membrane potential-dependences of the gating variables are given in Table 4.4.

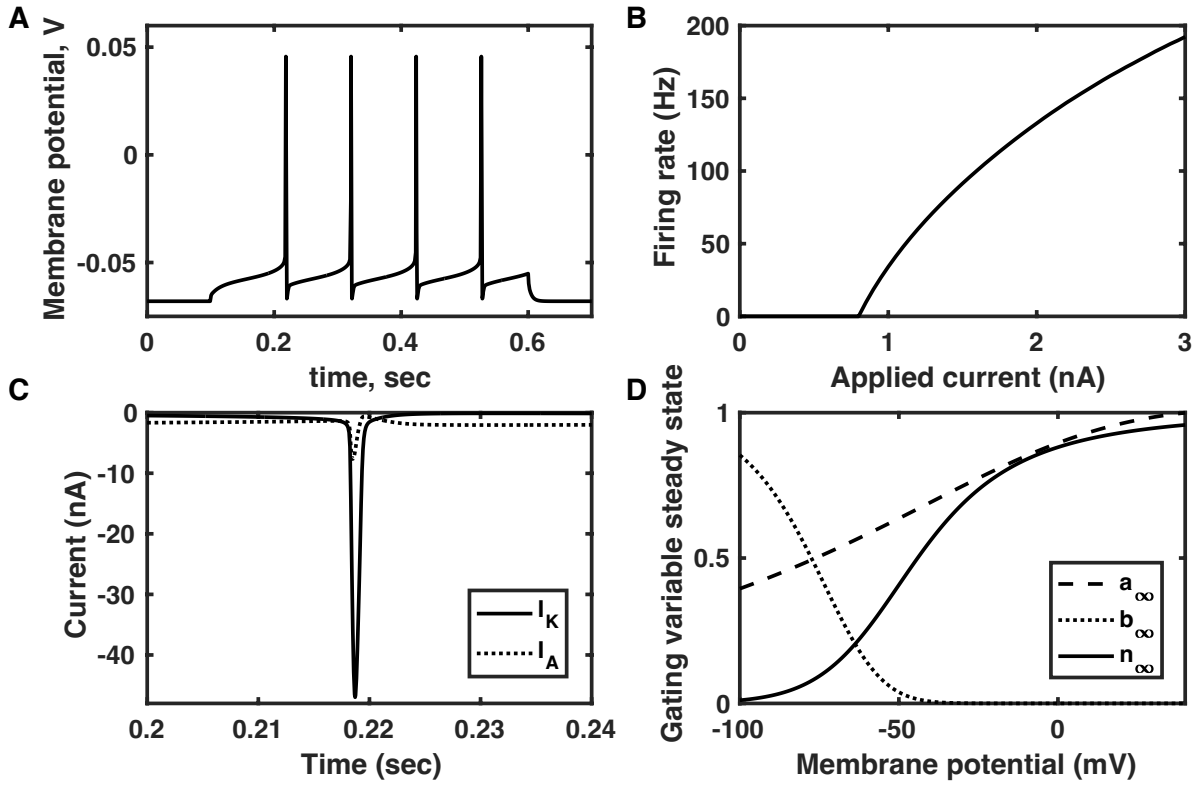

Figure 4.11. The Connor-Stevens model. A) The spike train with an applied current of 850pA between $t = 0.1$sec and $t = 0.6$sec. The delay to first spike is typical of a Type-I model. **B)** Type-I behavior is further exemplified by the f-I curve, which increases from zero without any discontinuity of firing-rate. **C)** The A-current (I_A, dotted) becomes stronger than the delayed rectifier current (I_K, dashed) shortly after a spike. Deinactivation of the *outward* A-current (b↑) counteracts deinactivation of the *inward* sodium current (h↑), preventing the rebound that causes oscillations in the membrane potential and Type-II behavior. **D)** Steady states of the gating variables show that at low membrane potential the conductance of the A current can remain high (both a_∞ and b_∞ are non-zero at $V = -70$mV). Hyperpolarization can even cause the steady-state of the A-type conductance to increase via deinactivation (b_∞ rises) while the conductance of the delayed rectifier current falls dramatically via deactivation (n_∞ falls). This figure is produced by the online code `CS_figure.m`.

These functions are incorporated in the online codes. The sodium and potassium gating variables are qualitatively similar to those of the Hodgkin-Huxley model. The steady states of the A-current gating variables are shown in Figure 4.11. Their time constants are sigmoid functions, dropping to the value given by the first term at high membrane potential and increasing by the amount on the numerator of the second term as the membrane potential is decreased to hyperpolarized levels.

The attentive reader may wonder why the reversal potential of A-type channels differs from that of potassium channels, because we showed in Section 2.1 that the reversal potential depends on the type of ion flowing through a channel—and the A-type current is a potassium current. There are two reasons for such differences. First, ion channels are not 100% specific—a smaller flow of other ions, at a level that is channel-specific, does shift the reversal potential for a given channel-type. Second, when optimizing a model of a neuron, it may be beneficial to be a little bit off in one parameter in order to make the model's behavior more realistic overall. In that sense, the "incorrect" parameter is accounting for many other variables not included explicitly in the model.

Like the sodium current, the A-current is a window current because it has both activation and inactivation variables. The "window" of membrane potential at which the A-current is active is slightly lower than that of the sodium channel, so that after a spike the A-current is slightly active (Figure 4.11C). Since the A-current is hyperpolarizing, its post-spike conductance acts to prevent a rebound spike that is typical of Type-II behavior.

Box 4.18. Signal processing pathways: chains of biochemical reactions, often involving activation of proteins via phosphorylation, or the reverse, which mediate a cell's response to an incoming signal.

Box 4.19. Endoplasmic reticulum: An extensive sub-compartment with relatively high calcium concentration, which pervades the cell, connecting to the nucleus and separated from the cytosol by a membrane with active channels.

Box 4.20. Mitochondria: Small sub-compartments with relatively high calcium concentration, which reside throughout the cytosol, most notable for producing ATP, the cell's energy supply.

Box 4.21. Cytosol: The aqueous part of the cytoplasm, the fluid in the main cell body, within which the nucleus, mitochondria, the endoplasmic reticulum, and other organelles reside.

4.5. Calcium Currents and bursting

Calcium ions play a crucial role in a vast number of signal processing pathways in biology. They are involved in fertilization[8], the cell cycle[9], transcriptional regulation[10,11], muscle contraction[12], and have a number of functions specific to neurons including synaptic transmission[13] and synaptic plasticity[14,15] that we will cover in this book. Table 2.1 indicates that calcium is maintained at very low concentrations in the cytosol—the bulk of the intracellular fluid—compared to the extracellular medium. This might be a consequence of the relative insolubility in water of calcium salts (such as calcium phosphate or calcium carbonate) whose precipitation could be harmful to cell function. As well as in the extracellular medium, higher calcium concentrations can be found in internal stores, such as the endoplasmic reticulum and mitochondria[16]. Transient release of calcium from such stores can lead to quite exquisite and complex calcium dynamics within cells, including neurons[17].

Given the positive charge and low concentration of calcium ions in the cytosol, the opening of calcium channels in the cell membrane produces an inward current like the

sodium current. Many different types of calcium channel exist in neurons, with their different functions determined by a combination of their location and their dynamics. As with the sodium and potassium channels that we have considered already, the dynamics of a calcium conductance depends on a combination of the time constants for activation and inactivation and on the voltage-dependence of the steady states of these gating variables. For example, rapidly activating high-threshold calcium channels located near axon terminals are able to respond to action potentials in a timely manner and mediate the calcium influx needed to initiate the release of vesicles of neurotransmitter[18,19] (see Chapter 5).

In the remainder of this chapter we will consider calcium channels with sufficient spatial spread that they can impact the membrane potential of the entire cell, leading to positive feedback in the same manner as a sodium spike. Indeed, we will see that calcium spikes are possible via a positive feedback process equivalent to the one that produces sodium spikes. The main difference being that a calcium spike follows slower dynamics than does a sodium spike, lasting tens to hundreds of milliseconds rather than one millisecond or less. If we consider that a calcium spike could be represented by a broad peak of applied current in our prior models, we see that the opening of calcium channels can lead to a burst of high frequency sodium spikes, which lasts until the calcium channels close.

Box 4.22. Calcium spike: A broad positive spike in the membrane potential that can last hundreds of milliseconds, wrought by positive feedback of voltage-gated calcium channels, which provide an inward current.

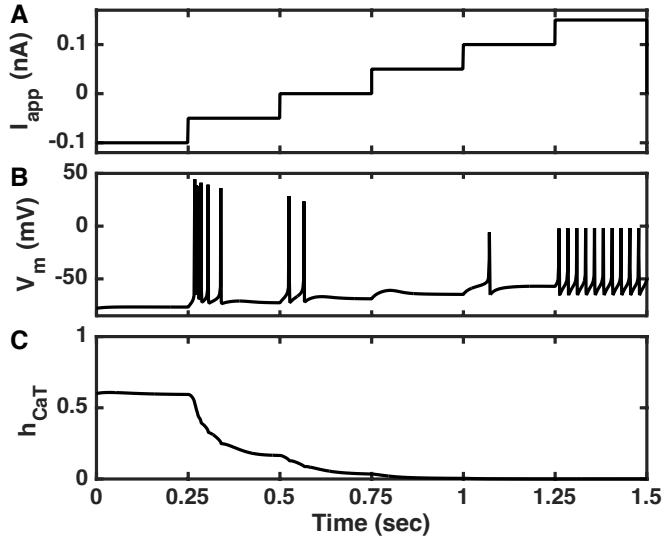

Figure 4.12. Deinactivation of T-type calcium channels produces post-inhibitory rebound. A) The current is stepped up every 250ms from an initial inhibitory current of -100pA in increments of +50pA. **B)** The membrane potential responds to the first step up to -50pA with a burst of 5 spikes, but does not respond with a spike following the 3rd step from 0pA to +50pA. With higher currents the neuron responds with regular (tonic) spikes. **C)** The inhibitory currents cause deinactivation of T-type calcium channels (a rise in h_{CaT}) allowing for the Ca^{2+} current to flow following hyperpolarization (left) but not depolarization (right). For parameters, see Tutorial 4.2.

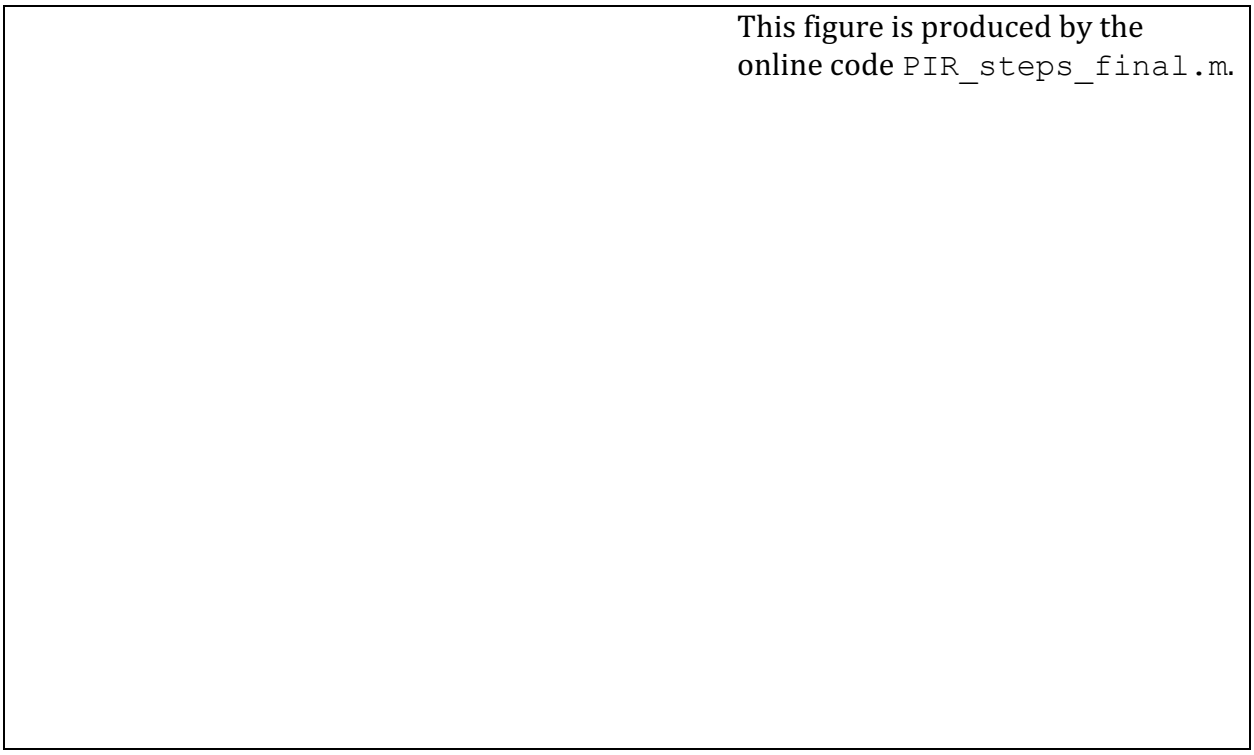

Box 4.23. T-type calcium channel: A voltage-gated calcium channel, which deinactivates at membrane potentials below rest, such that it supplies inward current following periods of release from hyperpolarization.

Box 4.24. Post-inhibitory rebound: A positive rebound in the membrane potential following a period of inhibition (similar to "anode break"), which can result from the deinactivation of T-type calcium channels.

4.5.1. Thalamic rebound and the T-type calcium channel

T-type calcium channels are low-threshold calcium channels that respond to periods of hyperpolarization with deinactivation, which allows them to open more easily following release of inhibition—via a post-inhibitory rebound—than without such inhibition. The channels are partially responsible for the pacemaking properties of heart tissue[20]. They are also found in thalamo-cortical "relay" neurons[21,22].

Thalamo-cortical neurons reside on the pathway between sensory receptors (as in the retina of the eye), which respond directly to external input, and neurons in sensory cortex, whose responses depend as much on the internal circuitry molded by prior experience. The behavior of the thalamo-cortical neurons is very different during sleep when we are less attentive to external inputs than during wakefulness. These differences in behavior can be attributed in part to the properties of the T-type calcium channels, which enable the neuron to switch between a depolarized tonic mode and a hyperpolarized bursting mode (see Figure 4.12). In the tonic mode during wakefulness, the firing rate of the neuron is approximately a monotonic function of the inputs at that time. In the bursting

mode during sleep, the neuron is mostly unresponsive to inputs, but produces intermittent bursts of high-frequency spikes.

Box 4.25. Tonic mode: A state of neural activity with relatively regular spiking, with spike rate varying monotonically with input current.

Table 4.5. Parameter values for Thalamic rebound model (Figure 4.12 and Tutorial 4.2).

Parameter	Symbol	Value *
Leak conductance	G_{Leak}	10nS
Maximum sodium conductance	$G_{Na}^{(max)}$	3.6μS
Maximum delayed rectifier conductance	$G_{K}^{(max)}$	1.6μS
Maximum T-type calcium conductance	$G_{T}^{(max)}$	0.22μS
Sodium reversal potential	E_{Na}	55mV
Potassium reversal potential	E_K	$-$90mV
Calcium reversal potential	E_{Ca}	120mV
Leak reversal potential	E_L	$-$70mV
Membrane Capacitance	C_m	100pF
Applied current	I_{app}	Variable

* Assumes a total membrane area of 0.01mm^2.

Table 4.6. Gating variables of the Thalamic rebound model (Figure 4.12 and Tutorial 4.2).

Gating variable	Steady state	Time Constant	Voltage-dependent variables
m	$\frac{\alpha_m}{\alpha_m + \beta_m}$	0	$\alpha_m = \frac{10^5(V + 0.035)}{1 - \exp[-100(V + 0.035)]}$ $\beta_m = 4000 \exp\left[\frac{-(V + 0.06)}{0.018}\right]$

h	$\frac{\alpha_h}{\alpha_h + \beta_h}$	$\frac{1}{\alpha_h + \beta_h}$	$\alpha_h = 350\exp[-50(V + 0.058)]$ $\beta_h = \frac{5000}{1 + \exp[-100(V + 0.028)]}$
n	$\frac{\alpha_n}{\alpha_n + \beta_n}$	$\frac{1}{\alpha_n + \beta_n}$	$\alpha_n = \frac{5 \times 10^4 (V + 0.034)}{1 - \exp[-100(V + 0.034)]}$ $\beta_n = 625\exp[-12.5(V + 0.044)]$
m_T	$m_{T,\infty}$	0	$m_{T,\infty} = \frac{1}{1 + \exp\left[\frac{-(V + 0.052)}{0.0074}\right]}$
h_T	$h_{T,\infty}$	τ_{h_T}	$h_{T,\infty} = \frac{1}{1 + \exp[500(V + 0.076)]}$ $\tau_{h_T} = 0.001\exp[15(V + 0.467)]$ if $V < -0.080$ $\tau_{h_T} = 0.028 + 0.001\exp\left[\frac{-(V + 0.022)}{0.0105}\right]$ if $V \geq -0.080$

4.6. Tutorial 4.2. Postinhibitory rebound.

Computational Goal: More practice writing and using a function; analyzing responses to variations of multiple parameters, and plotting functions of 2 parameters.
Neuroscience Goal: Understand the relationship of calcium conductance to bursting behavior and post-inhibitory rebound.

In this tutorial, you will produce a model thalamo-cortical neuron with a T-type calcium current. You will assess its response to single steps of applied current of variable size and baseline. You should simulate the neuron within a function rather than within a script, so that different levels of baseline current and step current can be manipulated in a separate file. You will find that storing separate aspects of the code in separate files makes for a neater, less cluttered set of codes that are easier to manipulate.

You will be simulating the following four dynamical equations of the model neuron:

$$C_m \frac{dV}{dt} = G_L(E_L - V) + G_{Na}^{(max)} m^3 h(E_{Na} - V) + G_K^{(max)} n^4 (E_K - V) + G_T^{(max)} m_T^2 h_T (E_{Ca} - V) + I_{app}$$

$$\frac{dh}{dt} = \alpha_h(1 - h) - \beta_h h$$

$$\frac{dn}{dt} = \alpha_n(1 - n) - \beta_n n$$

$$\frac{dh_T}{dt} = \frac{h_{T,\infty} - h_T}{\tau_{h_T}}$$

Parameters are given in Table 4.5. The activation functions for the sodium and the T-type calcium current are not included as dynamical equations because they are assumed

to respond instantaneously to changes in the membrane potential: $m = m_\infty = \frac{\alpha_m}{\alpha_m + \beta_m}$ and $m_T = m_{T,\infty}$. In this example, it is the long time constant for inactivation of the calcium current that will produce a slow timescale for burst duration. Membrane potential-dependence of all the gating variables are given in Table 4.6.

a) Produce a function "PIR" to be saved in the file "`PIR.m`", which simulates the model neuron described above for a period of 750ms. You will find the voltage-dependence of the gating variables already encoded in the online file "`PIR_Vdependence.m`," so you can copy expressions from that file if you prefer, instead of typing them out.

A baseline current and current step will be supplied to the function as its two inputs. The applied current should be set to the baseline value from 0-250ms, increased by the current step value in the mid-portion of the trial from 250-500ms, and returned to the baseline value from 500-750ms. The function should return two outputs: the membrane potential as a function of time and the time vector.

b) Produce a code that loops through a range of values for the baseline current (between −200pA and +200pA) and a range of values for the current step (between 0 and +100pA) added to each baseline current. For each pair of the parameters (the baseline current and the current step), calculate the total number of spikes produced during the current step and, if two or more spikes are produced, calculate the minimum inter-spike interval. Use "`imagesc`" or another graphics tool for plotting functions of two variables (*e. g.* see also "`surf`" or "`mesh`" or "`plot3`") to plot the total number of spikes on one graph and the minimum ISI on another graph, with baseline current on the x-axis and current step on the y-axis. Comment on your results and plot some examples of membrane potentials for each qualitatively distinct type of behavior.

4.7. Modeling multiple compartments

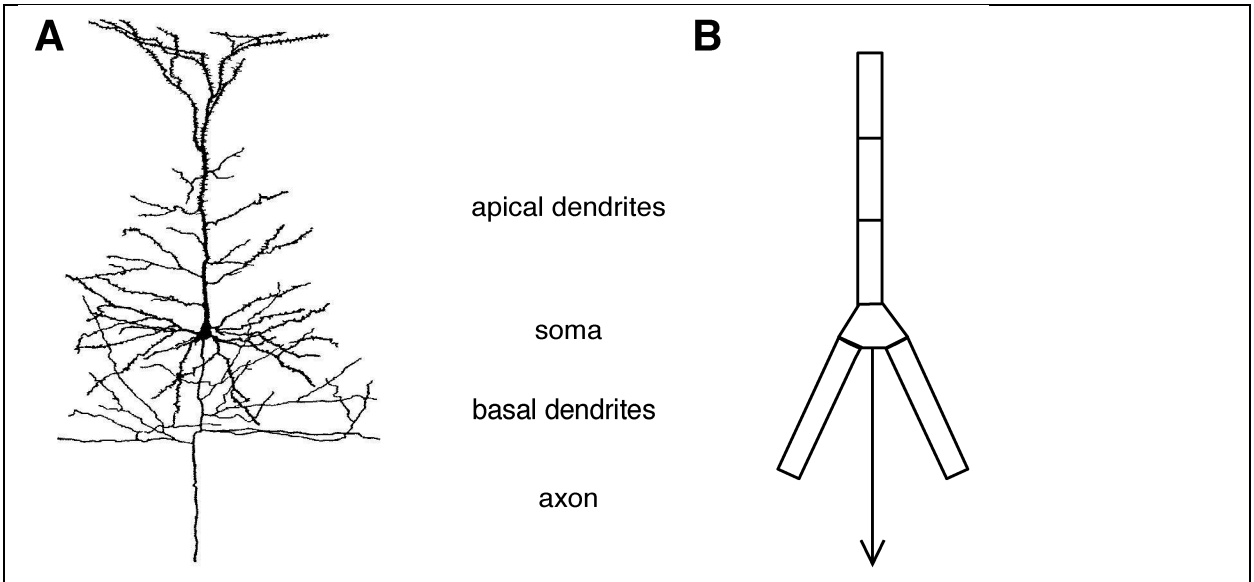

Figure 4.13. Simplifying a pyramidal cell with a multi-compartmental model. A. The traced structure of a pyramidal cell with a long apical dendrite with a large fraction of the cell's surface area at the top and other basal branches leaving the soma at the bottom. **B.**

The dendritic structure is modeled as 5 separate compartments connected either to each other or to the soma's separate compartment. The axon is often not modeled, because once the action potential is generated in its initial segment (which is typically incorporated in the soma in a model) the axon simply transmits the spike with minimal attenuation or modulation. This image first appeared as Figure 2.1 in the Book of Genesis, published under the GNU Free Documentation License, and was kindly provided by Prof. Dave Beeman, University of Colorado at Boulder.

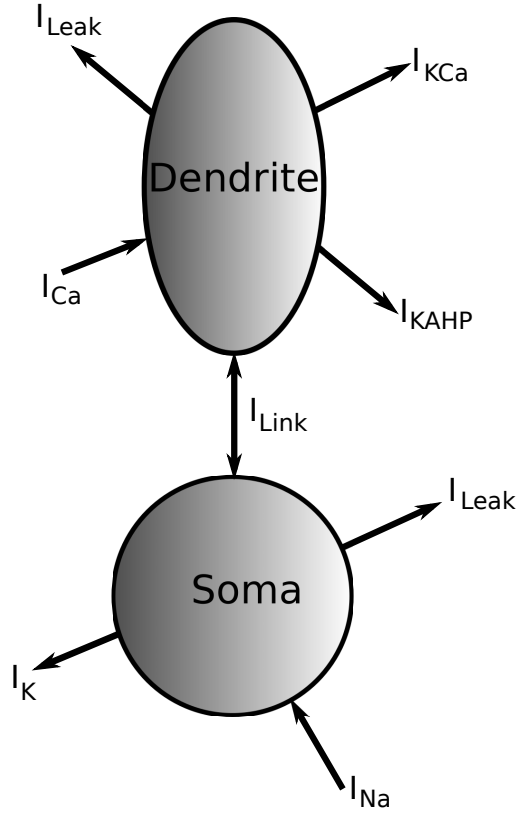

Figure 4.14. The Pinsky-Rinzel model is a two-compartment model of a bursting neuron. The two compartments with their intrinsic currents are shown. The soma is similar to the standard Hodgkin-Huxley model with an inward fast sodium current (I_{Na}), an outward delayed rectifier potassium current (I_K), as well as a small leak current (I_{Leak}) that is mostly outward. The two compartments are connected by an electrical resistor, which conveys a link current (I_{Link}) that flows from the compartment with higher membrane potential to the one with lower membrane potential at a given time. The dendritic compartment receives inward calcium current (I_{Ca}), whose activation provides the positive feedback needed to generate a dendritic calcium spike. The outward calcium-dependent potassium current (I_{KCa}) is relatively fast and can terminate a dendritic spike, whereas the outward after-hyperpolarization current (I_{KAHP}) is slower and largely determines the interval between dendritic spikes. The dendritic compartment has its own small leak current (I_{Leak}).

Up until now, we have ignored any impact of the spatial dependence of the membrane potential of a neuron. Such spatial dependence is important when the ion channel densities or the inputs a neuron receives vary across the neuron's membrane. Using a multi-compartment model, we can take into account some of the heterogeneity in the density of ion channels in different parts of a neuron and begin to understand how a neuron might respond differently to input currents depending on which part of the neuron receives the input.

The idea of a multi-compartmental model is to represent different sections of the neuron by individual compartments (Figure 4.13), each of which is ascribed a single time-varying membrane potential. Resistors are included between the compartments to connect them in a similar morphology to that of the original cell. If the compartments are carefully chosen, the extensive spatial structure of a neuron can be simulated in a manner that

captures the important characteristics of the original cell more fully than any of the single compartment, "point" neuron models that we have seen so far.

Several software packages exist for producing and simulating multi-compartmental models. The most common examples include Neuron, Genesis, and Brian. For a more complete introduction to multi-compartmental modeling, I recommend the Book of Genesis[23], from which Figure 4.13 is reproduced.

4.7.1. The Pinsky-Rinzel (PR) model of an intrinsic burster

As well as those neurons that produce bursts of spikes transiently upon depolarization, many others produce bursts rhythmically without the need for any external current. Such intrinsic, rhythmic bursters (sometimes called pacemaker neurons) can drive a complete circuit in a periodic pattern, or act as a time signal to separate different phases of neural processing or coordinate information transfer.

Box 4.26. Intrinsic burster: A neuron that fires bursts of rapid action potentials periodically, without external input.

Neurons can fire spikes intrinsically (*i. e.,* without external input) if excitatory channels begin to activate at low membrane potentials, so that no depolarization is necessary. For an intrinsic burster, it is the calcium current that has such a low threshold for activation.

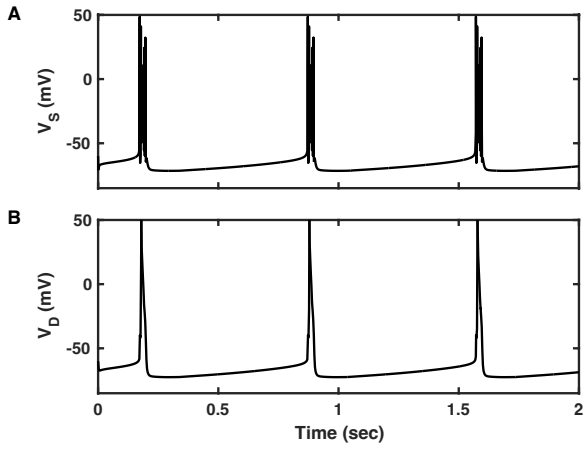

Figure 4.15. Intrinsic bursting in a variant of the PR model. Top. The somatic membrane potential produces bursts of high-frequency sodium spikes with an interval of hundreds of ms between bursts. **Bottom.** The dendritic membrane potential produces regular broad calcium spikes that are essential for the bursts in the soma. Parameters are given in Table 4.7 and equations for rate constants of gating variables in Table 4.8. The code used to produce this figure can be found online as `PR_euler_final.m`.

To simulate an intrinsically bursting neuron, we turn to a two-compartment model (Figure 4.14), in which the membrane potential of a somatic compartment is treated as distinct from the membrane potential of a dendritic compartment. The two-compartment model (the Pinsky-Rinzel model[24]), it should be noted, is itself a great simplification of a 19-compartment model (the Traub model[25]) of a pyramidal neuron found in the hippocampus of the guinea pig. However, the two-compartment model reproduces the key features of the more intricate Traub model (see Figures 4.15 and 4.16), and as we shall see is plenty complicated enough (Eqs. 4.19-4.20). Moreover, as an introduction to multi-compartmental

modeling, it contains the key features that can be built upon if more compartments are needed.

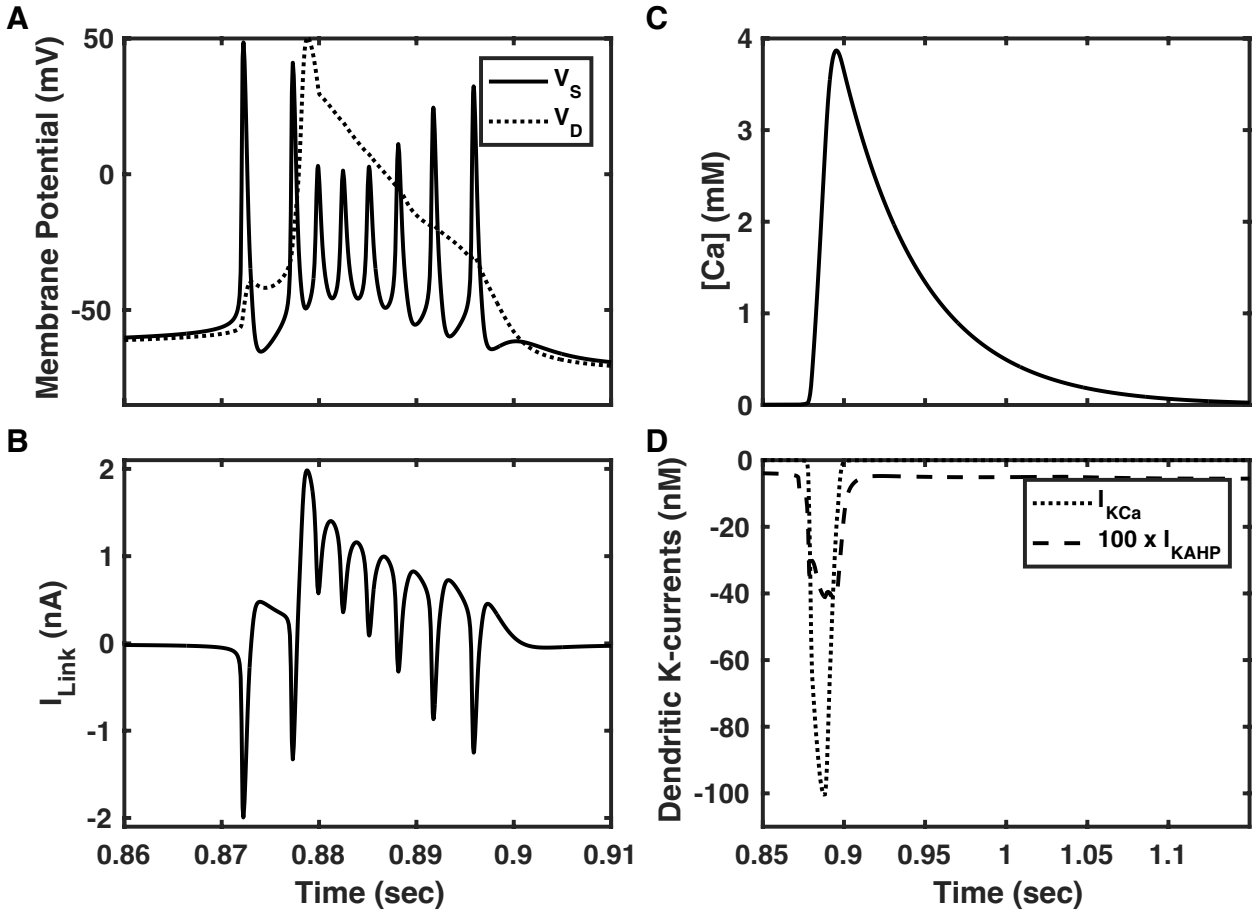

Figure 4.16. Dynamics of a single burst. A) In this burst, 8 sodium spikes (solid line) occur within 25ms. The first sodium spike produces a subthreshold potential rise in the dendrite (dotted line). The second sodium spike initiates a full, broad calcium spike in the dendrite. During the calcium spike the sodium spikes are rapid and do not return fully to baseline. As the calcium spike decays the frequency of sodium spikes gradually decreases until the end of the burst. **B)** I_{Link} is the current from the dendritic to somatic compartment. During a burst, there can be a "ping-pong" effect, a shuttling of current back and forth between the two compartments. In this example, the burst is initiated with a net flow of current from soma to dendrite ($I_{Link} < 0$), while during the burst the prolonged calcium spike in the dendrite produces a net current flow from dendrite to soma ($I_{Link} > 0$). **C)** Intracellular calcium rises dramatically within a burst and decays between bursts. (Note the extended timescale compared to A & B). **D)** Hyperpolarizing potassium currents activate during the burst. The faster, calcium-activated potassium current, I_{KCa}, which is also voltage-dependent, brings about the termination of the burst. The slower after-hyperpolarization current, I_{KAHP}, is also calcium-dependent, and after a burst must decay sufficiently before the next burst can

commence. Parameters are those of Figure 4.14. The code used to produce this figure can be found online as `PR_euler_final.m`.

4.7.2. Simulating the Pinsky-Rinzel model

The dynamical equations for the somatic (V_S) and dendritic (V_D) membrane potentials in the PR model are:

$$C_S\frac{dV_S}{dt} = G_{Leak}^{(S)}(E_L - V_S) + G_{Na}^{(max)}m^2h(E_{Na} - V_S) + G_K^{(max)}n^2(E_K - V_S) + G_{Link}(V_D - V_S) + I_{app}^{(S)} \quad \text{Eq. 4.19}$$

$$C_D\frac{dV_D}{dt} = G_{Leak}^{(D)}(E_L - V_D) + G_{Ca}^{(max)}{m_{Ca}}^2(E_{Ca} - V_D) + G_{KCa}^{(max)}m_{KCa}X(E_K - V_D) + G_{KAHP}^{(max)}m_{KAHP}(E_K - V_D) - G_{Link}(V_D - V_S) + I_{app}^{(D)} \quad \text{Eq. 4.20}$$

where C_S and C_D are the capacitances of each compartment, $G_{Leak}^{(S)}$ and $G_{Leak}^{(D)}$ the leak conductances, G_{Link} the conductance connecting compartments and $G_{Na}^{(max)}$, $G_K^{(max)}$, etc. are the maximal values of the corresponding active conductances. The gating variables vary with time according to the somatic membrane potential (m, h, n), or dendritic membrane potential (m_{Ca}, m_{KCa}), or the calcium concentration (X, m_{KAHP}). The dynamics of these gating variables is given in Table 4.8. Apart from the calcium-dependent term, X, which contributes to I_{KCa} (Figure 4.14) and responds instantaneously, the dynamics of all other gating variables are based on the usual rate constants, α and β. The membrane-potential dependences (and for m_{KAHP}, the calcium-dependences) of these rate constants are given in Table 4.8 and are returned by the two functions "`PR_soma_gating`" and "`PR_dend_gating`", which can be found in the online material.

Table 4.7. Parameter values used for intrinsic bursting in Figures 4.14 and 3.15.

Parameter	Symbol	Value
Fractional area of Soma	A_S	$1/3$
Fractional area of Dendrite	$A_D = 1 - A_S$	$2/3$
Somatic leak conductance	$G_{Leak}^{(S)}$	$A_S \times 5\text{nS}$
Dendritic leak conductance	$G_{Leak}^{(D)}$	$A_D \times 5\text{nS}$
Maximum sodium conductance	$G_{Na}^{(max)}$	$A_S \times 3\mu\text{S}$
Maximum delayed rectifier conductance	$G_K^{(max)}$	$A_S \times 2\mu\text{S}$
Maximum calcium conductance	$G_{Ca}^{(max)}$	$A_D \times 2\mu\text{S}$
Max. calcium-dependent potassium conductance	$G_{KCa}^{(max)}$	$A_D \times 2.5\mu\text{S}$

Max. after-hyperpolarization conductance	$G_{KAHP}^{(max)}$	$A_D \times 40\text{nS}$
Link conductance	G_{Link}	20nS
Sodium reversal potential	E_{Na}	60mV
Calcium reversal potential	E_{Ca}	80mV
Potassium reversal potential	E_K	-75mV
Leak reversal potential	E_L	-60mV
Capacitance of soma	C_S	$A_S \times 100\text{pF}$
Capacitance of dendrite	C_D	$A_D \times 100\text{pF}$
Somatic applied current	$I_{app}^{(S)}$	0
Dendritic applied current	$I_{app}^{(D)}$	0
Calcium decay time constant	τ_{Ca}	50ms
Conversion from charge to concentration	k	$\frac{2.5 \times 10^6}{A_D}\ \text{MC}^{-1}$

The model also includes the dynamics of calcium concentration, which depends on the calcium current, I_{Ca}, via

$$\frac{d[Ca]}{dt} = -\frac{[Ca]}{\tau_{Ca}} + k \cdot I_{Ca},$$

where I_{Ca} is one of the dendritic currents given in Eq. 4.20: $I_{Ca} = G_{Ca}^{(max)} {m_{Ca}}^2 (E_{Ca} - V_D)$. The time constant for decay of calcium is given by $\tau_{Ca} = 50\text{ms}$ here (an alteration of the original PR model). The constant, k, is a geometry-dependent factor required to convert the total charge generated by the calcium current through the surface of the dendritic membrane into a molar ionic concentration (with units of moles/liter, M) within the volume of the dendritic membrane where the calcium-dependent potassium channels are located.

Table 4.8. Gating variables of the Pinsky-Rinzel model.

Gating variable	Steady state	Time Constant	Rate constants
m	$\frac{\alpha_m}{\alpha_m + \beta_m}$	$\frac{1}{\alpha_m + \beta_m}$	$\alpha_m = \frac{320 \times 10^3 (V_S + 0.0469)}{1 - \exp[-250(V_S + 0.0469)]}$ $\beta_m = \frac{280 \times 10^3 (V_S + 0.0199)}{\exp[200(V_S + 0.0199)] - 1}$
h	$\frac{\alpha_h}{\alpha_h + \beta_h}$	$\frac{1}{\alpha_h + \beta_h}$	$\alpha_h = 128\exp\left[\frac{-(V_S + 0.043)}{0.018}\right]$ $\beta_h = \frac{4000}{1 + \exp[-200(V_S + 0.020)]}$

n	$\frac{\alpha_n}{\alpha_n + \beta_n}$	$\frac{1}{\alpha_n + \beta_n}$	$\alpha_n = \frac{16 \times 10^3 (V_S + 0.0249)}{1 - \exp[-200(V_S + 0.0249)]}$ $\beta_n = 250\exp[-25(V_S + 0.040)]$
m_{Ca}	$\frac{\alpha_{m_{Ca}}}{\alpha_{m_{Ca}} + \beta_{m_{Ca}}}$	$\frac{1}{\alpha_{m_{Ca}} + \beta_{m_{Ca}}}$	$\alpha_{m_{Ca}} = \frac{1600}{1 + \exp[-72(V_D - 0.005)]}$ $\beta_{m_{Ca}} = \frac{2 \times 10^4 (V_D + 0.0089)}{\exp[200(V_D + 0.0089)] - 1}$
m_{KCa}	$\frac{\alpha_{m_{KCa}}}{\alpha_{m_{KCa}} + \beta_{m_{KCa}}}$	$\frac{1}{\alpha_{m_{KCa}} + \beta_{m_{KCa}}}$	If $V_D > -0.010$: $\alpha_{m_{KCa}} = 2000\exp\left[\frac{-(V_D + 0.0535)}{0.027}\right]$; $\beta_{m_{KCa}} = 0$ If $V_D \leq -0.010$: $\alpha_{m_{KCa}} = \frac{\exp\left(\frac{V_D + 0.050}{0.011} - \frac{V_D + 0.0535}{0.027}\right)}{0.018975}$ $\beta_{m_{KCa}} = 2000\exp\left[\frac{-(V_D + 0.0535)}{0.027}\right] - \alpha_{m_{KCa}}$
X	$\min(4000[Ca], 1)$	0	—
m_{KAHP}	$\frac{\alpha_{m_{KAHP}}}{\alpha_{m_{KAHP}} + \beta_{m_{KAHP}}}$	$\frac{1}{\alpha_{m_{KAHP}} + \beta_{m_{KAHP}}}$	$\alpha_{m_{KAHP}} = \min(20, 20000 \times [Ca])$; $\beta_{m_{KAHP}} = 4$

4.7.3. A note on multicompartmental modeling with specific conductances versus absolute conductances.

Many models are produced using specific parameters such as specific conductance (*i. e.,* conductance per unit area) and or specific capacitance (*i. e.,* capacitance per unit area). The reason for their use is that such specific properties are more universal, being independent of cell size (Section 2.3.1). In models with many compartments, a parameter such as the specific capacitance is constant.

If the mathematical equations are written and simulated using specific properties, then any current flow is given as current per unit surface area of the compartment into which it flows. Therefore, care is needed as while the sum of "link" currents between compartments of different surface areas is a conserved quantity—the current flowing out of one compartment flows into another—the current per unit area (specific current density) is not conserved when the two compartments have different areas. In particular, if current flows from a large compartment into a small compartment, the outflow is a small specific current density, whereas the inflow is much larger. In the equations, this is dealt with by dividing the link current into a compartment by the fractional area of each compartment.

On the other hand, if absolute conductance and capacitance are used in a model, then the value of these parameters for each compartment scales multiplicatively with the area of that compartment. In this case, currents are treated absolutely, so that current from A to B is the negative of the current from B to A (like the link currents of Eqs. 4.19-4.20).

4.7.4. Model complexity

In general, the number of compartments we add to a model should depend on the question we are trying to answer. For example, the interplay between compartments is essential to the bursting behavior of the neuron modeled by Pinsky and Rinzel. Therefore, a minimum of two compartments is necessary if we are to understand bursting in this type of neuron, even though regular, intrinsic bursting can be generated in a single compartmental model. Alternatively, if we are concerned about whether the spreading of inputs over multiple sub-branches of dendrites has the same impact on a cell as the clustering of inputs in a single sub-branch, then a model with many more compartments, which includes those sub-branches, is necessary.

While adding more compartments to a model can seem like adding more realism (as can adding more ion channels to a single compartment) and therefore be nothing but beneficial, the dangers are multifold:

1) With the addition of more unknown parameters, the model could behave almost in any manner desired, depending on the value of those parameters, and therefore become disprovable (which some find convenient!). Or to quote von Neumann "with four free parameters I can make an elephant, with five I can waggle its trunk".

2) The more parameters there are, the harder it is to completely test the dependence on and relevance of each parameter, so it is unclear what features are important.

3) The more variables there are, the harder it is to gain any insight—from a dynamical systems perspective (Chapter 7)—as to why the model acts the way it does. For example, it can be unclear how the different variables interact with and affect each other, in which case understanding the processes in question can become impossible.

In summary, to paraphrase Einstein, "we should make a model as simple as possible but no simpler".

4.8. Hyperpolarization-activated currents (I_h) and pacemaker control

Box 4.27. Hyperpolarization-activated current, I_h: A mixed-cation inward current, without inactivation, activated by hyperpolarization and deactivated by depolarization.

Until now, all of the voltage-gated conductance terms that we have considered include an activation variable that increases with depolarization. While some channels also included an inactivation term, which became more positive at hyperpolarized potentials, they always required a subsequent depolarization to admit current. Here we consider the behavior of a hyperpolarization-activated cation conductance, which admits an inward, depolarizing I_h-current, when—as its name suggests—the cell is hyperpolarized[26].

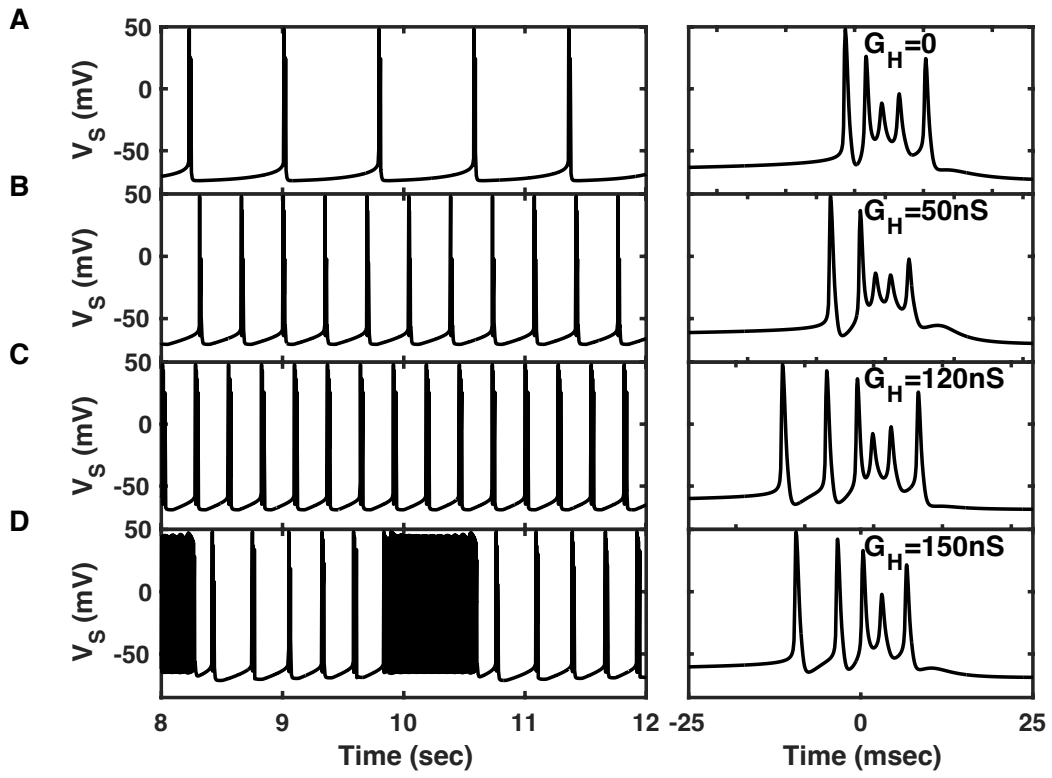

Figure 4.17. Impact of the hyperpolarization-activated current (I_h) on bursting. The somatic membrane potential of a simulated bursting neuron without I_h **(A)** more than doubles its burst frequency with little change in burst waveform when I_h is added with $G_h = 50$nS **(B)**, while the burst contains an extra pre-spike with increased I_h if $G_h = 120$nS **(C)**. For higher values of G_h **(D)**, regular bursting is lost with intermittent periods of prolonged high-frequency spiking. **Left:** 4 seconds of bursting activity shown. **Right:** A 50ms zoom-in of a burst, aligned to the upswing of dendritic membrane potential. This figure is produced using a modified PR model (Tables 3.8-3.9) with an additional I_h current produced using the method of Liu et al.[13] This figure is produced by the online code `IH_PR_loop.m`.

The I_h-conductance has no inactivation gating variable, just an activation variable, whose steady state increases monotonically with hyperpolarization. The channels allow a mixture of cations to flow through them, so the reversal potential, E_h, (-20mV in our model) is not as high as that of typical excitatory channels (see Table 4.9). We add I_h as a dendritic current to the PR model (Eq. 4.20),

$$I_h = G_h^{(max)} m_h (E_h - V_D), \qquad \text{Eq. 4.21}$$

where the dynamics of the activation variable, m_h, follow the usual form,

$$\frac{dm_h}{dt} = \frac{m_h{}^{\infty} - m_h}{\tau_{m_h}} \qquad \text{Eq. 4.22}$$

with

$$m_h{}^{\infty} = \frac{1}{1 + \exp[(V_D + 0.070)/0.006]} \qquad \text{Eq. 4.23}$$

and

$$\tau_{m_h} = 0.272 + \frac{1.499}{1 + \exp[-(V_D + 0.0422)/0.00873]}. \qquad \text{Eq. 4.24}$$

These functions are plotted in Figure 4.17.

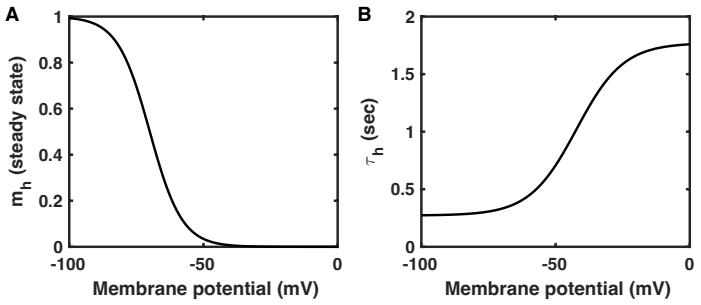

Figure 4.18. I_h gating variables. Left: Steady state of the activation variable, $m_h{}^{\infty}$, plotted from Eq. 3.23, increases from 0 to 1 with hyperpolarization between −50mV and −100mV. **Right:** Time constant for the I_h-conductance is in the 100s of ms, greater than typical burst durations. This figure was produced by the online code `IH_PR_loop.m`.

The I_h-conductance provides negative feedback, because it increases as the membrane potential gets lower, but acts to make the membrane potential higher. Unlike potassium activation and inactivation of sodium or calcium channels, both of which provide negative feedback to end a spike, the I_h-conductance helps with regeneration following a spike. In this sense, it is like deinactivation of sodium or calcium channels. Therefore, a major effect of increased I_h-conductance is a reduction of the inter-spike interval, or, more importantly in bursting cells, a reduction of the inter-burst interval[27] (see Figure 4.18). In this manner, the I_h-conductance may play a role in the homeostasis—*i. e.,* in the long-term control of the period—of bursting neurons (Section 8.6).

Table 4.9. Parameter values used for the burster with I_h current in Figure 4.17.

Parameter	Symbol	Value
Fractional area of Soma	A_S	1/3
Fractional area of Dendrite	$A_D = 1 - A_S$	2/3
Somatic leak conductance	$G_{Leak}^{(S)}$	A_S ×1nS
Dendritic leak conductance	$G_{Leak}^{(D)}$	A_D ×1nS
Maximum sodium conductance	$G_{Na}^{(max)}$	$A_S \times 3\mu$S
Maximum delayed rectifier conductance	$G_K^{(max)}$	$A_S \times 2\mu$S
Maximum calcium conductance	$G_{Ca}^{(max)}$	$A_D \times 2.5\mu$S

Max. calcium-dependent potassium conductance	$G_{KCa}^{(max)}$	$A_D \times 5\mu\text{S}$
Max. after-hyperpolarization conductance	$G_{KAHP}^{(max)}$	$A_D \times 60\text{nS}$
Max. hyperpolarization-activated conductance	$G_h^{(max)}$	0-200nS
Link conductance	G_{Link}	25nS
Sodium reversal potential	E_{Na}	60mV
Calcium reversal potential	E_{Ca}	80mV
Potassium reversal potential	E_K	-75mV
I_h reversal potential	E_h	-20mV
Leak reversal potential	E_L	-60mV
Capacitance of soma	C_S	$A_S \times 100\text{pF}$
Capacitance of dendrite	C_D	$A_D \times 100\text{pF}$
Somatic applied current	$I_{app}^{(S)}$	0
Dendritic applied current	$I_{app}^{(D)}$	0
Calcium decay time constant	τ_{Ca}	50ms
Conversion from charge to concentration	k	$\frac{1 \times 10^6}{A_D}\ \text{MC}^{-1}$

4.9. Dendritic computation

Neurons receive inputs at many thousands of distinct sites across their dendrites or cell body. In Chapter 5 we consider how to model these inputs, which arise due to activity in other neurons and appear at locations on the cell membrane called synapses where another neuron connects with the cell. In simple models, we just sum over individual inputs to obtain a total conductance or total current due to a particular kind of input. In these models the neuron performs a computation—which at a minimum is a nonlinear transformation—of its total input into a series of action potentials.

However, it is clear that in addition to the summed input, the relative location on the cell membrane of the different inputs is important[28]. In particular, if inputs are located near each other on the same dendrite they may generate a dendritic spike, in an example of supralinear summation[29]. The dendritic spike has a much stronger effect on the membrane potential of the soma than do those same inputs spread across multiple dendrites where they are locally too weak to generate a dendritic spike.

The generation of a dendritic spike can be thought of as a dendritic computation[30]—each dendrite acting as a local coincidence detector, producing a spike if it receives sufficient coincident excitatory inputs. In simplified models of complex, extensive neurons, as proposed by Bartlett Mel [31,32], the outputs of these dendritic computations provide the

inputs to the soma. The soma itself performs a computation on these inputs, emitting an action potential only when it receives sufficient dendritic input.

Figure 4.19 shows the response of a 4-compartment model neuron to different patterns of dendritic input. The model is based on the Pinsky-Rinzel model, but with the soma connected to three distinct dendritic compartments (for example representing an apical dendrite, D1, and two basal dendrites, D2 & D3). If a current of 75pA is applied simultaneously to each dendritic compartment (Figure 4.19B1-2) the cell's response is sub-threshold. However, if a current of 150pA is applied with the same temporal pattern to just one of the dendritic compartments (Figure 4.19C1-2) the resulting dendritic spikes produce regular spikes in the soma. This is noteworthy since the spike-producing total input to the cell in Figure 4.19C is 150pA, which is less than the subthreshold total input of 225pA used in Figure 4.19B. It is the higher local density of input that generates a neural response even when the cell's total input is lower.

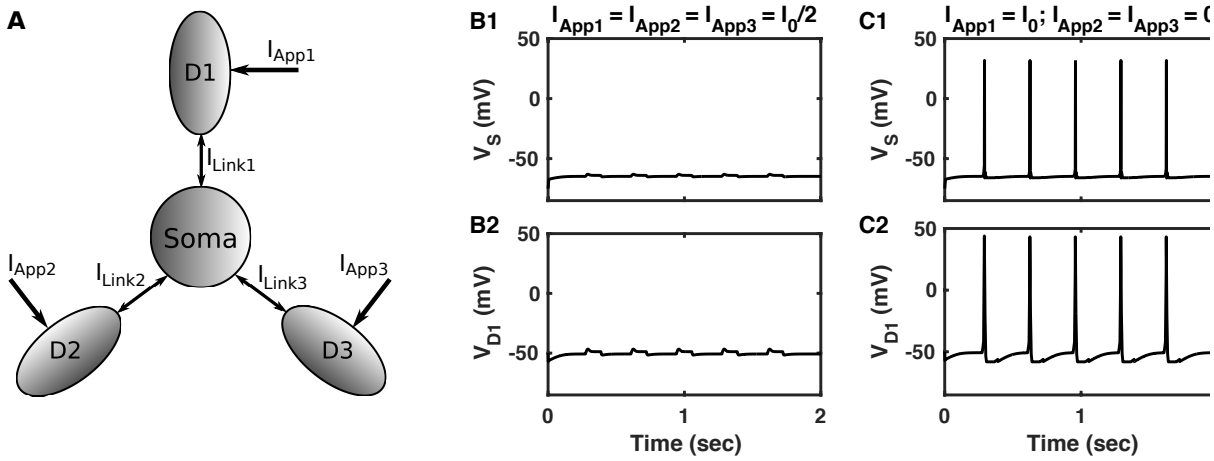

Figure 4.19. Neural activity depends on location of inputs. A. The model neuron is based on the Pinsky-Rinzel model (Fig. 4.13) but with three identical dendritic compartments (D1, D2, and D3) instead of just one. **B1, B2.** Response of the membrane potential in the soma (top) and apical dendrite (bottom), when regular pulses of applied current are injected simultaneously to all three dendritic compartments. **C1, C2.** Responses of the membrane potential in the soma (top) and apical dendrite (bottom) when 2/3 of the total current injected to the neuron in B is injected into a single dendritic compartment (the apical compartment, D1). This figure is produced by the online code `PR3branch.m`.

4.10. Tutorial 4.3. A two-compartment model of an intrinsically bursting neuron.

In this tutorial, you will simulate different variants of the two-compartment Pinsky-Rinzel model.

Neuroscience goal: Understanding how the two compartments affect each other and how bursting neurons respond to applied current.

Computational goal: Gain further familiarity with function calls. Producing histograms.

1) The functions "`PR_soma_gating`" and "`PR_dend_gating`", can be found in the online material in the file "`pm_functions.py`" within "`pm_package`". These can either be copied and pasted into your code, or you can download the folder "`pm_package`" with all of its contents and include directions at the top of your code to import the correct function as follows:

```
import sys
sys.path.insert(0,'/Users/YourUserName/YourFolder')
from pm_package.pm_functions import  PR_dend_gating, PR_soma_gating
```

where you replace " `/Users/YourUserName/YourFolder` " with whatever path is needed on your computer to reach the folder within which you placed "`pm_package`".

2) Generate a vector of values for the membrane potential (between -0.085V and 0.050V) and a vector of values for the calcium concentration (between 0 and 2×10^{-3}M). Use the downloaded functions to calculate and plot all 12 of the rate constants for gating variables on a suitable number of figures. (Hint: check the function "`PR_dend_gating.m`" in your editor to see how it works and the order of variables to be sent to it.)

3) Simulate the Pinsky-Rinzel model for 2s, using a timestep of 2μs, employing the same functions and parameters of Tables 4.7-4.8, except set $k = \frac{5\times10^{6}\ \mathrm{MC}^{-1}}{A_D}$ and $G_{Link} =$ 50nS.

4) Detect somatic spikes in your model by triggering a spike when the somatic membrane potential increases past -10mV and allowing a new spike to be triggered once a spike has ended only when the membrane potential decreases again to below -30mV.

5) Assess how the model's behavior depends on the strength of link between soma and dendrite by simulating the model with $G_{Link} = 0$nS, $G_{Link} = 10$nS, and $G_{Link} = 100$nS. Plot appropriate graphs to demonstrate the differences in behavior with changes in G_{Link}. Explain any changes in behavior and provide further graphs as evidence for your explanation where necessary.

6) For the intrinsic bursting model of 3), assess how the spiking behavior changes when a constant current is applied to the dendrite—try currents of 50pA, 100pA and 200pA. Carry out a similar assessment when the current is applied to the soma. Comment on any differences in behavior that arise when a current is applied to the soma rather than to the dendrite.

Questions for Chapter 4.

1) a) Explain the positive feedback involved in producing an action potential in the Hodgkin-Huxley model.
   b) Describe how three different terms produce negative feedback in the Hodgkin-Huxley equations.
2) In the Hodgkin-Huxley model, the potassium activation variable, n, impacts the conductance as n^4, which is equivalent to the effect of 4 independent subunits, with each one in the state necessary for channel-opening with probability, n. Would the exponent change from 4, and if so, in what direction, if the subunits were not independent, but had some degree of cooperativity to produce a positive correlation between their states? Explain your reasoning.
3) What is the key similarity between anode break in the Hodgkin-Huxley model and post-inhibitory rebound in the thalamo-cortical model neuron? What differences are there between the two?
4) If a model of a bursting neuron has too strong a calcium conductance, it may no longer produce a burst of sodium spikes, even though the soma has regular periods of what seems to be above-threshold depolarization. Why is this?

References for Chapter 4

1. Hodgkin AL, Huxley AF. A quantitative description of membrane current and its application to conduction and excitation in nerve. *J Physiol.* 1952;117(4):500-544.
2. Hodgkin AL, Huxley AF. The dual effect of membrane potential on sodium conductance in the giant axon of Loligo. *J Physiol.* 1952;116(4):497-506.
3. Hodgkin AL, Huxley AF. The components of membrane conductance in the giant axon of Loligo. *J Physiol.* 1952;116(4):473-496.
4. Hodgkin AL, Huxley AF. Currents carried by sodium and potassium ions through the membrane of the giant axon of Loligo. *J Physiol.* 1952;116(4):449-472.
5. Hodgkin AL, Huxley AF, Katz B. Measurement of current-voltage relations in the membrane of the giant axon of Loligo. *J Physiol.* 1952;116(4):424-448.
6. Hutcheon B, Yarom Y. Resonance, oscillation and the intrinsic frequency preferences of neurons. *Trends Neurosci.* 2000;23(5):216-222.
7. Connor JA, Stevens CF. Prediction of repetitive firing behaviour from voltage clamp data on an isolated neurone soma. *J Physiol.* 1971;213(1):31-53.
8. Whitaker M. Calcium at fertilization and in early development. *Physiol Rev.* 2006;86(1):25-88.
9. Skelding KA, Rostas JA, Verrills NM. Controlling the cell cycle: the role of calcium/calmodulin-stimulated protein kinases I and II. *Cell Cycle.* 2011;10(4):631-639.
10. Wiegert JS, Bading H. Activity-dependent calcium signaling and ERK-MAP kinases in neurons: a link to structural plasticity of the nucleus and gene transcription regulation. *Cell Calcium.* 2011;49(5):296-305.
11. Greer PL, Greenberg ME. From synapse to nucleus: calcium-dependent gene transcription in the control of synapse development and function. *Neuron.* 2008;59(6):846-860.
12. Jiang H, Stephens NL. Calcium and smooth muscle contraction. *Mol Cell Biochem.* 1994;135(1):1-9.
13. Jarvis SE, Zamponi GW. Masters or slaves? Vesicle release machinery and the regulation of presynaptic calcium channels. *Cell Calcium.* 2005;37(5):483-488.
14. Sjöström PJ, Nelson SB. Spike timing, calcium signals and synaptic plasticity. *Curr Opin Neurobiol.* 2002;12(3):305-314.
15. Zucker RS. Calcium- and activity-dependent synaptic plasticity. *Curr Opin Neurobiol.* 1999;9(3):305-313.
16. Verkhratsky AJ, Petersen OH. Neuronal calcium stores. *Cell Calcium.* 1998;24(5-6):333-343.
17. Ross WN. Understanding calcium waves and sparks in central neurons. *Nat Rev Neurosci.* 2012;13(3):157-168.
18. Stanley EF. The Nanophysiology of Fast Transmitter Release. *Trends Neurosci.* 2016;39(3):183-197.
19. Takahashi T, Momiyama A. Different types of calcium channels mediate central synaptic transmission. *Nature.* 1993;366(6451):156-158.
20. Mangoni ME, Couette B, Marger L, Bourinet E, Striessnig J, Nargeot J. Voltage-dependent calcium channels and cardiac pacemaker activity: from ionic currents to genes. *Prog Biophys Mol Biol.* 2006;90(1-3):38-63.

21. Destexhe A, Sejnowski TJ. The initiation of bursts in thalamic neurons and the cortical control of thalamic sensitivity. *Philos Trans R Soc Lond B Biol Sci.* 2002;357(1428):1649-1657.
22. Contreras D. The role of T-channels in the generation of thalamocortical rhythms. *CNS Neurol Disord Drug Targets.* 2006;5(6):571-585.
23. Bower JM, Beeman D. *The Book of GENESIS: Exploring Realistic Neural Models with the General NEural SImulation System, second edn.* Free internet ed. New York: Springer-Verlag; 1998, 2003.
24. Pinsky PF, Rinzel J. Intrinsic and network rhythmogenesis in a reduced Traub model for CA3 neurons. *J Comput Neurosci.* 1994;1(1-2):39-60.
25. Traub RD, Wong RK, Miles R, Michelson H. A model of a CA3 hippocampal pyramidal neuron incorporating voltage-clamp data on intrinsic conductances. *J Neurophysiol.* 1991;66(2):635-650.
26. Pape HC. Queer current and pacemaker: the hyperpolarization-activated cation current in neurons. *Annu Rev Physiol.* 1996;58:299-327.
27. Luthi A, McCormick DA. Periodicity of thalamic synchronized oscillations: the role of Ca2+-mediated upregulation of Ih. *Neuron.* 1998;20(3):553-563.
28. DeBello WM, McBride TJ, Nichols GS, Pannoni KE, Sanculi D, Totten DJ. Input clustering and the microscale structure of local circuits. *Front Neural Circuits.* 2014;8:112.
29. Wilson DE, Whitney DE, Scholl B, Fitzpatrick D. Orientation selectivity and the functional clustering of synaptic inputs in primary visual cortex. *Nat Neurosci.* 2016;19(8):1003-1009.
30. London M, Hausser M. Dendritic computation. *Annu Rev Neurosci.* 2005;28:503-532.
31. Poirazi P, Brannon T, Mel BW. Pyramidal neuron as two-layer neural network. *Neuron.* 2003;37(6):989-999.
32. Jadi MP, Behabadi BF, Poleg-Polsky A, Schiller J, Mel BW. An Augmented Two-Layer Model Captures Nonlinear Analog Spatial Integration Effects in Pyramidal Neuron Dendrites. *Proc IEEE Inst Electr Electron Eng.* 2014;102(5).
33. Liu Z, Golowasch J, Marder E, Abbott LF. A model neuron with activity-dependent conductances regulated by multiple calcium sensors. *J Neurosci.* 1998;18(7):2309-2320.